PROTON CONDUCTIVITY STUDIES OF ZIRCONIUM SILICATE/IONIC LIQUIDS MEMBRANES FOR PEM FUEL CELLS APPLICATIONS

by

Rana Muhammad Nauman Javed

A Thesis Presented to the Faculty of the
American University of Sharjah
College of Engineering
In Partial Fulfillment
of the Requirements
for the Degree of

Master of Science in
Chemical Engineering

Sharjah, United Arab Emirates

December 2020

Declaration of Authorship

I declare that this thesis is my work and, to the best of my knowledge and belief, it does not contain material published or written by a third party, except where permission has been obtained and appropriately cited through full and accurate referencing.

Signed: Rana Muhammad Nauman Javed

Date: 20/12/2020

Approval Signatures

We, the undersigned, approve the Master's Thesis of Rana Muhammad Nauman Javed

Thesis Title: Proton Conductivity Studies of Zirconium Silicate/Ionic Liquids Membranes for PEM Fuel Cells Applications

Date of Defense: 17-December-2020

Name	**Signature**
Dr. Amani Al-Othman Associate Professor, Department of Chemical Engineering Thesis Advisor	
Dr. Paul Nancarrow Associate Professor, Department of Chemical Engineering Thesis Co-Advisor	
Dr. Yassir Makkawi Professor, Department of Chemical Engineering Thesis Committee Member	
Dr. Yehya El-Sayed Professor, Department of Chemistry Thesis Committee Member	
Dr. Sameer Al-Asheh Head Department of Chemical Engineering	
Dr. Lotfi Romdhane Associate Dean for Graduate Affairs and Research College of Engineering	
Dr. Sirin Tekinay Dean College of Engineering	
Dr. Mohamed El-Tarhuni Vice Provost for Graduate Studies Office of Graduate Studies	

Acknowledgment

In essence, all praises to Almighty Allah for giving me the strength and ability to complete this work and for all his blessings in every step of my life.

Second, I would like to express profound thanks to my noteworthy and honorable advisors Dr. Amani Al-Othman and Dr. Paul Nancarrow for their endless and persistent help and guidance throughout. I express gratitude toward them for their important remarks and consolations during the past two years.

Moreover, I would like to deeply thank Dr. Yehya El Sayed and Dr. Yassir Makkawi for their help, support, and valuable discussions and suggestions. I sincerely thank Eng. Najla for her lab help and valuable suggestions.

I deeply thank the American University of Sharjah (AUS) and Dr. Sameer Al-Asheh for providing me with Graduate Teaching Assistantship (GTA) and continuous help during my graduate studies.

Finally, I would like to warmly thank my beloved parents, my siblings, and my friends at the American University of Sharjah (AUS) for their endless love and support and non-stop encouragement throughout this research.

Dedication

To my beloved parents, family & friends …

Abstract

This work reports the synthesis of a novel, high-temperature composite membrane for proton exchange membrane (PEM) fuel cells. High-temperature operation (> 100^{o}C) is preferred in PEM fuel cells as it results in better water management and an enhancement to the overall kinetics of fuel cells' electrodes. The current state of the art Nafion membrane is not suitable for high-temperature operation as their proton conductivities decline drastically. Hence, a novel Nafion-free membrane, based on zirconium silicates (ZrSi) and ionic liquids (ILs) is described in this thesis. Proton-conducting ZrSi/IL composite membranes were synthesized via precipitation of ZrSi/IL within the pores of polytetrafluoroethylene (PTFE) at room temperature. Seven different ILs were investigated to produce ZrSi/IL modified materials with ILs content ranging from 0.56% to 32% by mass. Significant enhancements in proton conductivities were observed upon the addition of the IL to ZrSi. Electrochemical impedance spectroscopy measurements showed proton conductivity values in the range of 0.1-0.2 S/cm, exceeding that of the Nafion membrane. The modified ZrSi/IL samples were further investigated by thermogravimetric analysis (TGA), scanning electron microscopy (SEM), Fourier Transform Infrared Spectroscopy (FTIR), X-ray diffraction (XRD), and energy-dispersive X-ray spectroscopy (EDX). TGA analysis of the modified ZrSi/IL materials demonstrated an approximately 20% weight loss at around 500^{o}C. Water uptake analysis indicated that the new composite membrane could hold more than 50% by weight of water. SEM analysis showed the changes in particles' morphology of the modified ZrSi/IL. The interactions of ILs with ZrSi were studied using FTIR & XRD. Changes in the ZrSi/IL crystalline structures in comparison with pure ZrSi were observed. The samples processed at a high-temperature (200^{o}C) and exhibited a high proton conductivity in the order of 0.001 S/cm. Thus, the ZrSi/IL membranes reported in this work are very promising as proton conductors for high-temperature fuel cell applications.

Keywords: *Zirconium Silicate (ZrSi), Ionic Liquids (IL), Polymer electrolyte membrane fuel cells (PEMFCs), Proton conductivity (S/cm)*

Table of Contents

List of Figures

List of Tables

Nomenclature

AFC	Alkaline fuel cells
[BMIM][DCA]	1-Butyl-3-methylimidazolium dicyanamide
[BMIM][SCN]	1-Butyl-3-methylimidazolium thiocyanate
DMFC	Direct methanol fuel cell
[DEMA] [OMS]	Diethylmethylammonium methanesulfonate
[EMIM][OMS]	1-Ethyl-3-methylimidazolium methanesulfonate
[EMIM][ESO_4]	1-Ethyl-3-methylimidazolium ethyl sulfate
EIS	Electrochemical impedance spectroscopy
EDX	Energy-dispersive X-ray
FTIR	Fourier transform infrared spectroscopy
GLY	Glycerol
[HMIM][TCM]	1-Hexyl-3-methylimidazolium tricyanomethanide
MCFC	Molten carbonate fuel cells
PAFC	Phosphoric acid fuel cells
PEM	Polymer electrolyte membrane or proton exchange membrane
SOFC	Solid oxide fuel cells
SEM	Scanning electron microscopy
[TEMA][OMS]	Triethylammonium methanesulfonate
TGA	Thermogravimetric analysis
XRD	X-ray diffraction
ZrSi	Zirconium silicate

Chapter 1. Introduction

1.1. Overview

Air pollution triggered by excessive energy production and industrial activities is responsible for several negative impacts on human health and the environment [1]. The non-renewable energy sources have increased carbon dioxide (CO_2) emissions, hence, leading to global warming. Fuel cells are one of the available technologies that produce clean energy (if green hydrogen is the fuel) [2]. Fuel cells are defined as electrochemical devices (galvanic cells) that convert the chemical energy of a fuel (Liquid i.e. methanol, ethanol, and Gas i.e. hydrogen, alkanes) [3].

In the early history of the fuel cell, it was first known as the "gaseous voltaic battery" (Grove, 1842). It used hydrogen and oxygen as reactants with platinum-coated electrodes in the presence of sulfuric acid electrolyte [4]. In 1882, Lord Rayleigh developed a modified form to improve the efficiency of the platinum electrode by increasing the surface of action between the solid electrode, the gas, and the liquid [5]. In 1889, Ludwig Mond and Carl Langer carried an experiment to increase the "surface of action" of the cell with a porous matrix to contain the liquid electrolytes inside it [6]. Davtyan (1946) developed a high-temperature cell that would work at 700°C with a solid ionic conductor as the electrolyte. General Electric (GE) developed the first polymer electrolyte membrane (PEM) fuel cells in the early 1960s. Grubb and Niedrach (1960) developed a fuel cell with a solid ion-exchange membrane electrolyte based in cross-linked polystyrene with sulfonic acid (HSO_3) groups in 1960, but these were replaced by Nafion in 1966 [6]. Direct methanol fuel cells were developed by researchers (Hartnig and Jörissen) with aqueous acid electrolytes that would not react with the CO_2 produced in the electrochemical reaction [7].

Fuel cells can be categorized into five different types i.e. phosphoric acid, molten carbonate, alkaline, solid oxide, and polymer electrolyte or proton exchange membrane. Among all of them, Polymer electrolyte membrane or proton exchange membrane fuel cells (PEMFCs) received significant consideration in recent years because of their all-solid structure and good efficiency. PEMFC ordinarily work at temperatures ~ 80°C. Higher temperature operation has several advantages including high reaction kinetics, improvement of catalyst hindrance towards contaminants, and

the recuperation of reaction heat. The most commonly used membrane in PEMFCs is Nafion. The optimum temperature of this perfluorosulfonic acid film is about 80 ^{o}C with a proton conductivity of 0.1 S/cm and at fully hydrated conditions [8]. So, the temperature increases, Nafion dries out and its proton conductivity drastically decreases [9]. High-temperature operation is favored in PEMFCs for several reasons. It enhances electrodes' kinetics for the fuel cells, improves water management and the fuel cell tolerance for pollutants, such as carbon monoxide (CO), subsequently, permitting the utilization of a wider range of cheaper catalysts and fuels [10]. Unfortunately, an increase in the working temperature is not feasible with the utilization of Nafion membranes.

Most PEMFCs use hydrogen or methanol as fuel. The use of hydrogen as a fuel imposes several limitations including the energy density and storage pressure. Hydrogen is not readily available and is mostly produced by steam reforming of natural gas [11]. On the other hand, hydrocarbons have certain features like easy transportation and high energy storage density with well-defined infrastructures which can reduce the overall cost of PEMFCs by the removal of processing units for fuels. The advantages of hydrocarbons seem to be significant, but their rates of reactions are minimum at low temperatures [12]. Furthermore, as mentioned previously, Nafion membranes cannot operate at high temperatures. Therefore, there is a significant effort toward the development of a high-temperature membrane. High-temperature operations can reduce water accumulation at the cathodic site which can expose more surface area of catalyst for more movements of molecules for electrochemical reactions. It can also improve tolerance towards catalyst poisoning and CO impurities allowing the use of wider ranges of fuels or the use of less expensive catalysts. Henceforth, there is a huge exertion to grow high-temperature proton conducting membranes and the current conventional membrane in PEMs does not allow high-temperature operation.

In this thesis, a novel membrane has been evaluated as a high-temperature proton conductor. The membrane is composed of zirconium silicate, $ZrSiO_4$ (ZrSi) incorporated with ionic liquids (IL). Zirconium silicate has a mesoporous structure which has high thermal stability and promising proton conductivity. Ionic liquids are ionic compounds (salts) which are liquid below 100 ℃. More commonly, ionic liquids have melting points below room temperature. These are a special class of compounds

that contain organic cation and organic/inorganic anions. Some of the remarkable key features of ionic liquids are thermal and chemical stability, low melting point, high ionic conductivity, non-flammable, non-volatility, moderate viscosity, and high polarity [13].

1.2. Thesis Objectives

The present work aims at synthesizing a Nafion-free proton conducting material based on zirconium silicates (ZrSi) & ionic liquids for direct hydrocarbon PEM fuel cells. Direct hydrocarbon fuel types have been proposed for PEMFCs as hydrocarbons are less expensive and available with existing infrastructure and can be utilized to meet the electricity needs of commercial and industrial applications.

The primary objectives of this study are:

1. Synthesize proton conducting membranes based on zirconium silicate with a variety of ionic liquids (1-hexyl-3-methylimidazolium tricyanomethanide, diethylmethylammonium methanesulfonate, 1-butyl-3-methylimidazolium dicyanamide, 1-ethyl-3-methylimidazolium methanesulfonate, triethylammonium methanesulfonate, 1-ethyl-3-methylimidazolium ethyl sulfate, 1-butyl-3-methylimidazolium thiocyanate).
2. Study the effect of glycerol on proton conductivities of the best composite membranes electrolytes for direct hydrocarbon fuel cells.
3. Evaluation of the properties of the synthesized material including their proton conductivity via electrochemical impedance spectroscopy (EIS), surface morphology, chemical structure, and water uptake characteristics using various characterization techniques including Scanning electron microscopy (SEM), Fourier transform infrared spectroscopy (FTIR), X-ray diffraction (XRD), Energy dispersive X-ray (EDX) and thermogravimetric analysis (TGA).

1.3. Thesis Organization

The thesis has been divided into six chapters. Chapter one is related to the thesis introduction which includes an overview of the project, problem statements, and objectives of the study. Chapter two includes an extensive background and literature review about applications of different fuel cell types and direct hydrocarbon fuel cells (DHFC). It also provides information about the currently used proton conductors and

the suggested alternative electrolyte materials for PEM fuel cells, including zirconium silicate and ionic liquids. Chapter three deals with the materials and detailed experimental methodology used to carry out this project. Chapter four presents the experimental results of the study and the development of proton-conducting materials. It also provides a detailed analysis and discussion of the findings in this research. Chapter five presents the results and discussion for the incorporation of glycerol in the ZrSi material. Finally, Chapter six includes conclusions and recommendations for future work.

Chapter 2. Background and Literature Review

Chapter two discussed the fundamentals of fuel cells, and types of fuel cells used i.e. phosphoric acid fuel cell (PAFC), molten carbonate fuel cell (MCFC), alkaline fuel cells (AFC), solid oxide fuel cell (SOFC), and polymer electrolyte or proton exchange membrane fuel cell (PEMFC). Also, it concerns the general applications, hydrocarbons utilized in different fuel cell configurations, efficiency calculation & thermodynamics with the primary motivation of high-temperature fuel cell operations.

2.1. Fundamentals of Fuel Cells

The fuel cell working principle is that a fuel gas containing hydrogen, for example, methane, streams past the anode where an electrochemical reaction takes place which results in the production of electrons and H^+ ions (protons). The main purpose of the membrane in fuel cells (FCs) is to allow movement of proton conductance and to separate the cathode from the anode and prevent combustions. Figure 1 shows the basic operating principle of fuel cells. When the fuel is introduced at the anode (e.g. hydrogen), it is oxidized on the surface of the catalyst to produce electrons and protons. The electrons can flow externally toward the cathode. Oxygen from the air moves through the cathode where reduction of oxygen takes place with the help of incoming electrons. Negatively charged oxygen ions relocate through the electrolyte film react with the hydrogen to produce water, or CO_2 if there should arise an occurrence of methanol.

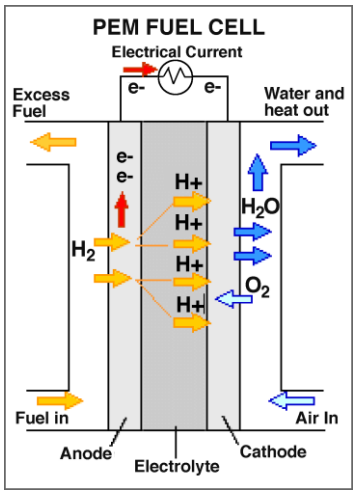

Figure 1: Basic operating principle of fuel cells [14]

This electrochemical reaction creates electrons, which move from the anode to an outside load and back to the cathode, finally both finishes the circuit, and electric power is supplied [15]. To build an output voltage, a few energy components are stacked together to frame the core of a clean power generator [16]. If the fuel is pure hydrogen, the following electro-oxidation reactions take place in the fuel cell as follows:

At the anode, pure hydrogen is oxidized and converted into H^+ ions (proton) with the release of electrons

$$2H_2 \rightarrow 4H^+ + 4e^- \quad (1)$$

At the cathode, oxygen is reduced with the help of electron provided by the anode and forms water with available H^+ ions (protons)

$$O_2 + 4H^+ + 4e^- \rightarrow 2H_2O \quad (2)$$

The overall reaction can be written as

$$2H_2 + O_2 \rightarrow 2H_2O \quad (3)$$

If the fuel is a hydrocarbon such as propane (C_3H_8) then the following reactions occur[17]:

Steam reforming takes place at the cathode in the very first step which results in carbon dioxide, protons, and electrons

$$C_3H_8 + 6\ H_2O \rightarrow 3\ CO_2 + 20\ H^+ + 20\ e^- \quad (4)$$

Oxygen is then reduced at the cathode:

$$5\ O_2 + 20\ H^+ + 20\ e^- \rightarrow 10\ H_2O \quad (5)$$

The overall reaction can be written as

$$C_3H_8 + 5\ O_2 \rightarrow 3\ CO_2 + 4\ H_2O \quad (6)$$

2.2. Types of Fuel Cells

Based on electrolyte employed, fuel cells are classified into five main categories: phosphoric acid fuel cell (PAFC), molten carbonate fuel cell (MCFC),

alkaline fuel cells (AFC), solid oxide fuel cell (SOFC), and polymer electrolyte or proton exchange membrane fuel cell (PEMFC).

2.2.1. Phosphoric acid fuel cell (PAFC). Phosphoric acid fuel cells are the most developed and commercialized types around the world [18]. The operating temperature is between 170°C and 210°C [19]. This temperature is higher than in proton exchange membranes fuel cells but lower than the operating temperature in molten carbonate fuel cells and solid oxide fuel cells [20]. It utilizes 100% liquid phosphoric acid (H3PO4) as the electrolyte. The anode is made of platinum/carbon encased with polytetrafluoroethylene (PTFE) and the cathode is made of 0.5 mg Pt/cm2 in a graphite structure [18]. High stability, moderate temperature operation, and a high tolerance for carbon dioxide are the key features of PAFCs [21]. The main disadvantages related to PAFCs are large warm-up time and the power density is 10 to 100 times lesser in comparison with ordinary combustion engines [22]. Anode poisoning is another disadvantage as PAFC anodes are made of noble metals i.e. platinum which is quite expensive and intolerant to CO. This makes it unacceptable for use in auto applications. Its operating efficiency is 36% to 42%.

2.2.2. Molten carbonate fuel cell (MCFC). Molten carbonate fuel cells are best suited for large stationary power generators. Molten carbonate fuel cells are best suited for large stationary power generators. They work at a high temperature, nearly 600^{o}C, so metallic cell components can be utilized by keeping the ionic conductivities in promising ranges [23]. They have a lower working temperature than the solid oxide fuel cell (SOFC) and they create steam that can be utilized to produce more power. A eutectic mixture of lithium and potassium carbonates are utilized as an electrolyte. Anode and cathode in MCFC are based on nickel and nickel oxide respectively [24]. Figure 2 shows the working of MCFC. Natural gas, bio-fuels, and coal fuels are several types of MCFC that have been used for commercial as well as industrial applications [15]. The advantages and disadvantages of MCFCs can be distinguished based on high working temperatures. Carbon capture and storage (CCS) make its use significantly in worldwide applications [25]. MCFC might be legitimately operated with hydrogen, carbon monoxide, petroleum gas, and propane. They do not need noble metal catalysts for electrochemical redox reactions. Additionally, they do not need any foundation improvement for establishment but a long time is expected to reach the working

temperature and producing power [26]. On the other hand, low power density, corrosion, and dissolution problems are the disadvantages of MCFCs which make their applications on limited scales [27].

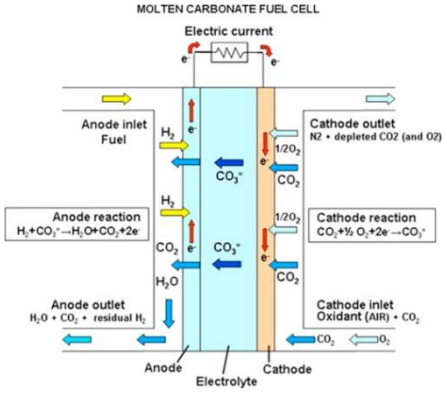

Figure 2: Working of MCFC [27]

2.2.3. Alkaline fuel cell (AFC). Alkaline fuel cells are one the oldest and the most cost-efficient type of fuel cells that usually operates at a low temperature of range of 60°C to 90°C with low catalyst consumption [15]. Figure 3 shows the working of the AFC. It uses hydrogen as fuel and potassium hydroxide as a liquid electrolyte due to its high conductivity [28]. Nickel catalyst is used for both anodic and cathodic reactions. The simple structure of the AFC eliminates the bipolar plates. The byproducts are water, electric sources, and heat which can be further used in many other applications. The main advantage of AFC is high electrical efficiency which is about 60% at a low operating cost [28]. The main reason for using an inexpensive catalyst is the fast reduction reaction of an anodic site in an alkaline medium [29]. On the other hand, catalyst poisoning with carbon dioxide (CO_2) is the disadvantage of AFC which can affect the performance drastically. The presence of CO_2 in AFC leads to a reaction between KOH which gives the potassium carbonate K_2CO_3 [30].

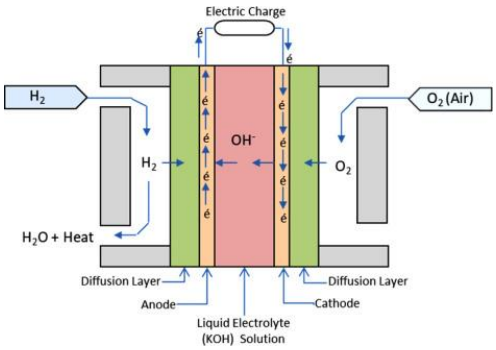

Figure 3: Working of AFC [31]

2.2.4. Proton exchange membrane fuel cell (PEMFC). Polymer electrolyte or proton exchange membrane fuel cell (PEMFC) is favorable among all other fuel cell types due to low-temperature operation between 60 and 100 °C, high power density, low maintenance cost, and quick start-up which makes them a significant clean and renewable technology [15][16]. The arrangements of the electrode assembly in PEMFCs are simpler than different sorts of fuel cells because of the robustness of the electrolyte. Moreover, they have a longer lifetime and less expensive to produce [32]. The principal components of PEM fuel cells are anode and cathode with the catalyst layer and an electrolyte. The fuel cell's stack is associated with series or parallel arrangements to produce the required voltage and current. The anode and cathode comprise the membrane electrode assembly (MEA) which involves a proton conducting membrane, catalyst layers, and permeable gas diffusion layers [33]. Catalytic layers can be made by platinum, permeable PVC, Ni-Br, Rainy Nickel or Teflon covered with silver contingent upon temperature necessities [34]. The most commonly used catalysts in PEMFCs are iridium, platinum, ruthenium, palladium, and gold [33]. Platinum (Pt) demonstrated better performance over different metals especially reduction reactions at cathode [35]. Besides the overall performance and superiority of metals, its high cost makes a restriction for the commercialization of PEM fuel cells [36]. Carbon monoxide is emphatically adsorbed on platinum active sites at low temperatures prompting the harming of the valuable Pt catalyst [37]. Several efforts have been made for the optimum size of the platinum catalyst. The high cost of catalyst, CO poisoning, and limited temperature operations are the disadvantages of PEMFC.

2.3. Applications of Fuel Cells

2.3.1. Portable power. Portable fuel cells are light-weight, long life-time, a versatile power source that eliminates the continual charging which prolongs the real-time application of a gadget [38]. In comparison, auxiliary (battery-powered) appliances have battery charger frameworks that comprise of AC chargers that require an outlet to be charged or DC chargers that will energize the batteries from another power source. Battery-powered devices are not functional for certain convenience since they can be weighty and not meet the force necessities. Some fuel cells applications incorporate workstations, phones, power devices, battery chargers, unattended sensors, and automated aeronautical and submerged vehicles [39]. A fuel cell needs a continuous

energy supply which is a remarkable contrast between battery-powered appliances. Some fuel types that have been utilized with fuel cells incorporate metal hydrides, methanol, acids, ethanol, and obviously, hydrogen. For compact fuel cells, methanol and ethanol can be provided to the power module as fuel or a fuel reformer can likewise be appended to the energy component bundle.

2.3.2. Stationary power applications. Fuel cells for fixed applications have been utilized economically for more than twenty years. The principle contrast in these fuel cells is fuel availability and proper stack design for heating and cooling conditions. Fuel cells can be utilized as the main power source. It is frequently used to supply power to houses that are not associated with the main power grid. In hybrid technology, fuel cells can be associated with photovoltaics, batteries, capacitors, or wind turbines, giving essential or auxiliary power. Energy components can likewise be utilized as a reinforcement or auxiliary power generator giving power when the system is down. Numerous manufacturers implemented fuel cells as a power station for automobile industries during the 1990s. Unlike other energy component applications, the fuel type frequently utilized is gaseous petrol. Other regular fuel types are propane, compacted hydrogen, biogas, methanol, oil-based energizes, and town gas, blend gas, digester gas, and landfill gas. The most well-known fixed energy component type is the Proton Exchange Membrane Fuel Cell (PEMFC), yet Solid Oxide Fuel Cells (SOFC), Molten Carbonate Fuel Cells (MCFC), Alkaline Fuel Cells (AFC), and Phosphoric Acid Fuel Cells (PAFC) have additionally been utilized [40].

2.3.3. Transportations. Fuel cell technology is one of the most efficient and cleanest power sources for transportation which can eliminate the frequent consumption of fossil fuels. Fuel cells supply a consistent measure of power which can be utilized as the auxiliary force source vehicle such as start-up and other power needs. The working temperature of a car fuel cell is between 60 to 80ºC because of the usage of the hydrated polymer layer, which restricts the temperature to below 100ºC. A fuel cell can easily replace the ordinary lead-acid batteries in utility vehicles that require operation maintenance and charging/discharging time. Like the fuel cell autos, the fuel type frequently utilized is compacted hydrogen, even though methanol, metal hydrides, and sodium borohydride have additionally been illustrated. The most widely recognized kind of power device utilized is the Proton Exchange Membrane Fuel Cell (PEMFC),

yet Direct Methanol Fuel Cells (DMFC) and Alkaline Fuel Cells (AFC) have likewise been utilized.

Table 1: Comparison of fell cell technologies [38]

Fuel cell type	Electrolyte	Temperature (°C)	Output (kW)	Efficiency %	Application
PEMFC	Solid organic polymer	50 - 100	<1-250	25-58	Backup power, Distribution
AFC	KOH (aqueous)	90 -100	10-100	60	Military space
PAFC	Liquid phosphoric acid	15-200	50-1000	>40	Distributed generation
MCFC	Liquid solutions of Li, Na and K carbonates	600-700	<1-1000	45-47	Large distributed generation
SOFC	Yttria stabilized zirconia	600-1000	<1-3000	35-43	Auxiliary power

2.4. Direct Hydrocarbon Fuel Cells

2.4.1. Significance of using direct hydrocarbon fuel cells. Fuel cells can be classified based on fuel used i.e. hydrogen, methanol, ethanol & propane, etc. Most commonly hydrogen is preferred in fuel cells due to large current densities and zero CO_2 emission compared to all other available fuel cells; however, it has transportation, storage, and flammability problems that make its use less preferable [41]. Steam reforming of natural gas followed by the water gas shift reaction is the main source of hydrogen production, which results in the emission of CO_2 as a byproduct [42]. Therefore, most hydrogen production still contributes significantly to carbon emissions.

Direct methanol fuel cell (DMFC) is another type of PEMFCs. It is reasonable because of low-temperature activity, long lifetime, and fast refueling framework qualities but

methanol is a corrosive hydrocarbon and requires a special fuel handling mechanism which increases the cost [43]. At the anode, methanol and steam are converted into carbon dioxide (CO_2), H^+ ions, and protons while at the cathode steam or water is formed using oxygen available in the air. The major problems in this methanol fuel cell are slow reaction rates at anode and methanol passage rate through membranes that lead to a decrease in the overall efficiency of fuel cells [44].

In this thesis, the hydrocarbon which is used in PEMFCs is propane which can be introduced easily to the anode where the electro-oxidation reaction takes place. The expense per-kWh conveyed from hydrogen produced from non-renewable energy sources is higher than the expense per-kWh when utilizing a hydrocarbon fuel straightforwardly in the fuel cell. Besides, the most basic route for delivering hydrogen is by utilizing an external reformer. In the reformer, the fuel chemically reacts with oxygen or water to produce H_2, CO, CO_2, N_2, and H_2O which builds the unpredictability and the expense of the fuel cell framework [45]. The main advantage of using hydrocarbons directly is to eliminate the fuel processor unit, minimize the overall cost, and remove greenhouse gases [46][47].

2.4.2. Types of Direct Hydrocarbon Fuel Cells

2.4.1.1. Hydrocarbons in polymer electrolyte fuel cells (PEMFCs). To get a high power density source at minimal environmental pollution with a solid framework, researchers have diverted their attention towards Polymer Electrolyte Fuel Cells (PEMFCs) [48]. PEM fuel cells can operate on various forms of fuels. Hydrogen is still more favorable than other fuels since running on hydrogen will create just water and the framework has high power density. In nature, hydrogen is always associated with some other forms and it needs to be extracted with existing technology. Firstly, hydrogen can be made via cracking of fossil fuel on the account of CO formations which is considered one of the cheapest sources for hydrogen production and provide an acceptable solution to balance the hydrogen economy. The second process is the most expensive which used an enormous amount of electrical energy i.e. electrolysis and is termed as "zero carbon emission."

Hydrocarbons are an alternative to hydrogen which can be utilized directly into a fuel cell or by conversion to H_2 with a reformer. Hence, they will lead to a decrease in the overall operational cost of fuel management in fuel cells [49]. On a basic level,

propane is cheap and has more power density than hydrogen. In 1960, Savadogo demonstrated a low-temperature direct propane polymer electrolyte membrane fuel cell (DPFC). The propane was injected directly into a fuel cell. The membranes were Nafion 117 doped with heteropolyacids (HPAs) or poly-benzimidazole (PBI). The anode depended on platinum, platinum-ruthenium, or platinum-chromium oxide electro-catalysts and the cathode depended on a platinum electro-catalyst. Results indicated that polymer electrolyte layers can be easily taken care of by propane gas to make direct propane fuel cell (DPFC). This has numerous focal points contrasted with methanol, for example, lower cost, vast working temperature ranges, ease of handling, less complicated infrastructure, and higher power density than those of methanol. The main disadvantage in DPFC likewise is carbon dioxide [50]. Another alternative to hydrogen is methanol which also displays promising power density. Direct methanol fuel cells (DMFCs) are not considered to be efficient in comparison with propane due to their lower efficiency but it can generate a significant amount of energy.

The negative aspect of using DMFCs is CO emission which can poison the Pt catalyst and decrease the surface area available for reactions and hence leading to a decrease in overall cell potential. The possible solution to minimize the poisoning is to add another metal like Ru to Pt catalyst with can be helpful in CO oxidations. Methanol crossover is the main obstruction in low efficiency which can be reduced by polymeric materials or by membrane grafting [51]–[53].

2.4.1.2. Hydrocarbons in alkaline fuel cells (AFCs). One of the best and most efficient fuel cell technologies is alkaline fuel cell which has wide industrial, military, and space applications, especially in NASA. Alkaline fuel cells (AFCs) have gained attention due to their good O_2 reduction reactions in the basic medium in comparison with an acidic one at a low operational cost with higher efficiency than other fuel cell types [54] The most commonly used fuels in AFCs are hydrogen, low hydrocarbons (methanol and ethanol), and sodium borohydride. Koscher [55] carried out an experimental study with the help of fuel (methanol) and electrolyte (KOH) with platinum electro-catalytically active carbon electrodes which was resulted in a current density of 2 mA cm^{-2}. Methanol crossover was minimized by the addition of a third grid electrode named platinum-catalyzed nickel which resulted in a better current density of 6 mA cm^{-2}. Prabhuram [56] also studied methanol oxidation in KOH

electrolytic fuel cell type with platinum electrodes with a variation in methanol and KOH ratios. Sodium borohydride is another best alternate for fuels in AFC as it oxidizes to hydrogen via a two-step reaction at high temperature and pH of less than 7 [57]. Direct glucose is another potential source of fuel for AFC as it is abundantly present which can be converted to hydrogen by some controlled chemical reactions but its applications are limited due to the unavailability of a cost-effective anode catalyst. Gao and Liu [58] investigated direct glucose alkaline fuel cells (DGAFC) with nickel-cobalt composite catalyst and modified activated carbon anode. The highest power density came out to be 23 mA cm^{-2} with a molar ratio of (1:3) between glucose and KOH.

2.4.1.2. Hydrocarbons in phosphoric acid fuel cells (PAFCs). Low temperature fuel cells had gained popularity in the 1960s which involved operation with hydrogen and oxygen with ion-exchange mediums or KOH solutions as the electrolyte. Hydrogen was not commercially available at that era, and, hence caused the operational barrier to the operation of the fuel cell. Steam reforming was another option for hydrogen production with hydrocarbons. So, an electrolyte with non-volatile nature and operations low to medium temperature led to the invention of phosphoric acid fuel cells (PAFCs) [59]. In alkaline fuel cells, KOH can react with carbon dioxide leading to the formation of K_2CO_3 which makes its application lesser than other fuel cells. On the other hand, PAFC uses 100% ortho-phosphoric acid as an electrolyte in the presence of platinum and carbon electrode assembly. Propane is the most widely used fuel in PAFCs due to high rates of chemical reactions. Petroleum diesel, biodiesel, and n-hexadecane can be used as direct hydrocarbons with phosphoric acid fuel cells [60].

2.4.1.3. Hydrocarbons in solid oxide fuel cells (SOFCs). Solid oxide fuel cells are highly energy-efficient fuel cell technologies that can also operate large temperature ranges with direct hydrocarbons involving higher hydrocarbons [61]. They can also operate with hydrogen and ammonia, but due to storage and transportation limitations, they are not fully commercialized. They do not need any reformer for the conversion of fuel, hence, the overall operational cost is minimized in SOFCs. Moreover, special electrodes are utilized that can be stable mechanically and chemically at high-temperature operations.

As fuels are injected at the anodic side of SOFC for oxidations, they need to be stable for different types of fuels for high-temperature operations. Ordinary SOFCs contain

Ni-based anode as it has high electrochemical stabilities but it has some limitations i.e. carbon deposition on the surface of the catalyst which minimizes overall cell performances [62]. H_2S is another important issue related to the usage of direct hydrocarbons and is considered to be harmful to SOFC as well [63]. To overcome the main problems, various solutions have been studied and experimented with different anode and fuel performances. Gorte and Kim [64] investigated Cu-CeO_2 based anode since Cu has good resistance towards the coke deposition. Recently, Ding and Tao carried out a study on ceramic anode material for direct hydrocarbons SOFCs. $SFNM_2O$ (double perovskite structure) showed very good power densities of 520 mW cm^{-2} for H_2 & 380 mW cm^{-2} using CH_4 as fuel. Also, sulfur problems in SOFCs can be minimized by using Cu-ceria-YSZ anodes [65].

2.5. Fuel Cell Efficiency Calculations

The fuel cell efficiency can be calculated by using the ratio between the electrical power output and the fuel input [66]:

$$\eta = \frac{Electrical\ power\ output\ (P_{fc})}{Fuel\ input\ (F_{in})} \tag{7}$$

At standard conditions, the free energy of water formation is[67]

$$H_2 + ½\ O_2 \rightarrow H_2O_{(l)} \qquad \Delta H_f = -285.84\ kJ/mol$$

The free energy (ΔG) can be calculated by subtraction of the total enthalpy (ΔH) and irreversible entropy changes ($T\Delta S$), i.e.

$$\Delta G = \Delta H - T\Delta S \tag{8}$$

The theoretical potential corresponding to the ΔG at atmospheric pressure and a temperature of 25ºC has a value of 1.229 so the equation $\eta = \frac{V}{1.482}$ will have a value of 1.229/1.482 = 0.83 which shows the theoretical efficiency for a hydrogen fuel cell is 83%.

For propane C_3H_8 based hydrocarbon fuel cell:

- Anode: $C_3H_8 + 6H_2O \rightarrow 3CO_2 + 20e^- + 20H^+$ $E_o = 0.137$ V (9)
- Cathode: $5O_2 + 20e^- + 20H^+ \rightarrow 10H_2O$ $E_o = 1.229$ V (10)
- Overall: $C_3H_8 + 5O_2 \rightarrow 3CO_2 + 4H_2O$ $E_{cell} = 1.092$ V (11)

The values of ΔG = -2107 kJ and ΔH = - 2219 kJ, hence, the fuel cell efficiency can be calculated by the second law of efficacy as follows:

$$\eta = \frac{\Delta G}{\Delta H} = \frac{-2107}{-2219} = 0.95$$

The above efficiency calculations depict that direct hydrocarbon (propane) fuel cells have higher efficiency than hydrogen fuel cells which can be further improved. Electro-catalyst surfaces of the anode electrodes can also be improved to increase the overall efficiency of direct hydrocarbon PEMFC [68].

2.6. Motivation for High-Temperature Operations

The proton exchange membrane (PEM) is the main element in a fuel cell which separates the mixing of reactants and prevents combustion as well as maintaining an electrical path for an external load. This peculiar characteristic makes its usefulness, properties, cost, and overall reliability very prominent for real cell working. Primary characteristics for PEMFC should be reasonable proton conductivity (preferably higher than 10^{-4} S/cm [69]) that can be achieved by maintaining reasonable hydration levels in the membrane. This will provide proton hopping sites. Also, high mechanical and chemical strength (over long periods) in an emphatically oxidative condition are the goals of PEMFCs [70].

PEM fuel cells are limited in their operating temperatures since a certain amount of water needs to be retained in the electrolyte membrane for proton hopping via hydrogen bond interactions to provide optimum conductivity. The high current density operation tended to dehydrate the membrane i.e. as more protons cross the membrane, they take water molecules with them to the cathode, which resulted in reduced conductivity (Electro-osmotic drag). At low temperatures, flooding problems arise due to the accumulation of water molecules at the cathodic site which reduces the passage of incoming oxygen from the air. Hence, it causes back diffusion of water from the cathode to the anode. When it operates at high temperatures, water molecules will not accumulate at the cathode so more molecules can diffuse for the reaction at a more exposed area of catalyst that usually are the major problems of low-temperature PEMFC can be avoided.

The main problem in direct hydrocarbon (propane) fuel cell is the lowest current density and the value obtained with the Pt electrode was reported to be less than 2 mA/cm^2 at 0.2 V [50]. The proton movements are increased as the temperature increases, which will result in a more effective kinetic reaction in the fuel cell.

The following key points emphasize the importance of high-temperature fuel cells operations:

- Fuel cell temperature operation over 100^oC is of great importance because anode catalyst poisoning by CO is less significant. The energy of fuel oxidation will be improved and the proficiency of the cell altogether can be upgraded. CO deposition on the catalyst surface can be reduced by increasing the temperature [71]. Moreover, reduction in the overall cost of expensive catalysts and minimization of electrode flooding are the main advantages of operating at high temperatures. Also, higher temperature operation would allow the use of less expensive catalysts.

- High-temperature operation is beneficial as it leads to better water management at the cathodic side and also for the recovery of heat produced which is superseded by the large exposed surface area of a catalyst which allows more diffusion for more reaction.

- The overall kinetics of gas transportation can be enhanced by carefully choosing a proton conductivity membrane that can carry water contents at this high temperature. It decreases the issues of humidification in the fuel cell stack hence over fuel cell performance can be increased [72]. A proton-conducting membrane based on a poly-benzimidazole (PBI) membrane doped with phosphoric acid (PA) can work up to 200^oC [10].

2.7. Thermodynamics of PEM Fuel Cells

Thermodynamics is utilized to understand the energy changer in fuel cells. The performance of any type of fuel cell relies upon thermodynamic changes. The heating value of a fuel is given by the enthalpy. Not all heating potential of fuel can be utilized to perform helpful work; the reversible work of fuel is characterized by Gibbs's free energy, which is the electrical work. The investigation of the electrical impacts shows that the electrochemical reactions of the fuel utilized are relative to the electric flow

and the reversible work is corresponding to the reversible voltage. The cell voltage fluctuates with temperature, weight, and reactant/product regimes. Irreversible losses have effects on reversible and real procedures [73]. Nernst potential for H_2 and several other hydrocarbons had been studied in the past to evaluate conversion on the equilibrium potential. It has been reported that in the case of hydrogen, the potential drops by 15% while hydrocarbons are utilized, the potential drops just by 1% over a similar conversion for n-butane [65]. Due to the properties of easy storage and overall cost, hydrocarbons are more preferable than hydrogen in fuel cells as hydrogen needs an enormous amount of energy for its production from hydrocarbons [45].

One of the best methods for the determination of the performance of any type of fuel cell is a plot between potential output in volts versus the current density loadings (mA/cm^2) which is also known as polarization curve. The ideal fuel cell potential is equivalent to the thermodynamic value i.e. V = 1.23 V but the actual cell potential is always decreased from its ideal potential because of several types of irreversible losses which are called polarization or over-potential. Any type of fuel cell polarization curve is divided into three different regions i.e. activation, ohmic, and concentration as shown in Figure 4.

Activation polarization is the first region where the charge transfer processes take place during the electrochemical reactions on electrode sites (surface phenomenon). At a low current density, cell potential mainly drops due to overcoming the restriction of Brownian electric current and ions. These losses are associated with slow kinetics on electrode surfaces and depend on the nature of the type of electrode, ionic interactions, ion-solvent interactions, and the electrode-electrolyte interface [74].

Ohmic polarization or over-potential is the second region that occurs at moderate current densities and cell potential decrease linearly with current densities. These losses are due to a combination of mainly three types of resistance i.e. resistance in the electrolyte, resistance to the flow of electrons at the electrode side, and contact resistance at the cell terminals [43]. These losses depend on materials selection, stack geometry, and temperature.

Concentration polarization or mass transport over-potential is the third region. To maintain the efficiency of the fuel cell, continuously be supplied with fuel and

oxidant with continuous removal of products are required. This polarization occurs due to a decrease in concentration gradient (reactant at the electrode-electrolyte interface and product accumulation at cathode sides) which ultimately leads to a decrease in cell potential. It can be decreased by optimizing the mass transport in the fuel cell electrodes and flow structures.

The final voltage is between 0.5 and 1.0 V lower than the thermodynamic voltage (E_{therm}) which is given by the following equation [75]:

$$E = E_{therm} - \eta_{act} - \eta_{ohm} - \eta_{conc.} \quad (12)$$

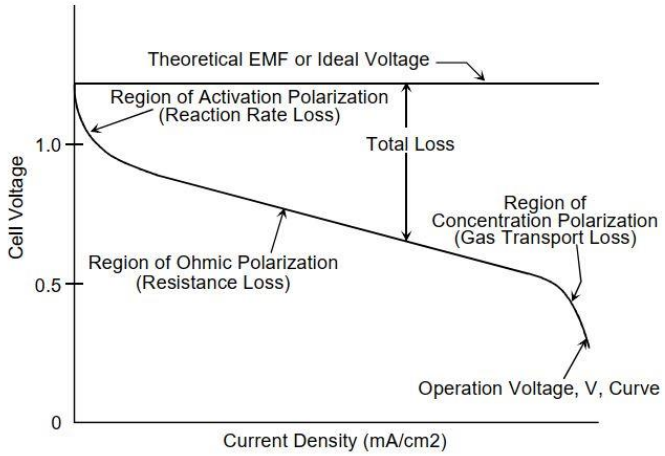

Figure 4: Polarization curve [76]

2.8. Membranes for PEM Fuel Cells

The performance of a proton exchange membrane fuel cell (PEMFC) is largely determined by the membrane-electrode assembly (MEA) which is composed of an anode for fuel oxidation, a cathode for oxygen reduction, and a proton-conducting membrane for proton transportation. Water is required as the charge carrier for the proton conductivity inside the Nafion membrane. Nafion was developed by DuPont in the 1960s [77].

Water management plays an important part in PEMFCs operations. Low water quantities will lead to membrane dehydration, consequently increase the cell resistance and cause the proton conductivity of the membrane to decrease. On the other hand, an excessive amount of water on the cathode side will cause flooding and the transportation of oxygen through the porous gas diffusion electrode will be restricted.

The sulfonated hydrocarbon polymer membranes are available which possess a good thermo-mechanical quality at a low cost. In any case, these sulfonated, perfluorinated, or non-fluorinated membranes have a few inconveniences: they should remain a certain amount of humidity to accomplish high proton conductivity.

Polytetrafluoroethylene (PTFE) is one of the most widely used synthetic polymer that has a melting point of around 327°C and good heat resistance. Furthermore, it has high flexural strength, hydrophobic (water-resistant) nature and its low ion exchange capacity (IEC) shows high proton conductivity at high temperatures. Moreover, this unique fluorocarbon polymer structure is responsible for good mechanical and chemical stability. On the other hand, polyethersulfone is a good candidate for membrane due to its thermal as well as mechanical stability at high temperatures.

The development of inorganic-organic composite membrane had been proposed by several researchers such as fluorinated polymer/SiO_2 composite, Nafion/PTFE/zirconium phosphate ($Zr(HPO_4)_2$) composite, Nafion/TiO_2 composite, PVA/SiO_2/silico-tungstic acid composite, Nafion/SiO_2 composite, sulfonated poly(ether sulfone) (SPES)/boron phosphate, (BPO_4) composites [78]. Essentially, it is still the advancement of a proton exchange membrane that fulfills all the necessities specifically, the proton conductivity sufficiently high at high temperature, strength, mechanical and electrochemical stability at an economic price for PEMFCs.

Table 2: Membranes Overview in PEMFCs [73]

Types	Structure	Advantages	Disadvantages
Perfluorinated	• Fluorinated backbone • Fluorocarbon side chain • Ionic clusters consisting of sulphonic acid ions attached to side chains	• Mechanical and chemical stability in oxidative and reductive environments • Good proton conductivity	• Expensive • Temperature limitation (80^oC)

Partially fluorinated	• Fluorocarbon base • Hydrocarbon or aromatic side chain grafted onto the backbone	• High mechanical strength, chemical, and thermal stability as compared to Perfluorinated	• Fast degradation • Low durability
Non-fluorinated	• Modified Hydrocarbon or aromatic base, with polar parts	• Low cost • Proton conductivity comparable to Nafion • Chemically and thermally stable at high temperatures	• Low durability • High swelling
Ionic liquid	• organic cation /organic, inorganic anion	• High conductivity • High thermal stability	• Membrane construction problems

2.8.1. Zirconium silicate ($ZrSiO_4$) Zirconium silicate ($ZrSiO_4$) is a compound known as zirconium ortho-silicate. It is usually colorless, insoluble in water, acids, alkali, which occurs in nature as mineral zircon. It has a tetragonal crystalline structure with silicon and oxygen. It is found in nature-in acidic volcanic rocks, through the fusion of zirconium dioxide (ZrO_2) & sand (SiO_2) structure. Synthetic zirconium-based ion exchangers have gained attention because of their selectivity, good ion-exchange behavior, and some important chemical applications like the ion-exchange membrane [79]. Several synthesis methods are accounted for including non-thermal synthesis of mesoporous zirconium silicate, microporous zirconium silicates with atomic layer structure of zirconium silicate films utilizing zirconium tetra-tert-butoxide and silicon tetrachloride (substitutional reactions). It has been found that zirconium silicate has high melting points (2550 ^oC) as compared to other compounds containing silicon and its production cost is also low as the source [80]. Zirconium silicate has high thermal stability up to 400^oC with a very low percentage of weight loss. Moreover, the proton

conductivity (1.45 x 10^{-3} S/cm) for pure ZrSi was reported. Figure 5 shows crystalline structure of ($ZrSiO_4$).

Zirconium silicate is produced by precipitation reaction with sodium silicate (Na_2SiO_3) and zirconium oxychloride ($ZrOCl_2$). The precipitation reaction of ZrSi proceeds according to the following equation [81]:

$$Na_2SiO_3 + ZrOCl_2 \rightarrow ZrSiO_4 + 2NaCl \quad (13)$$

2.8.2. Ionic liquids. Ionic liquids (IL) are a special class of compounds that mainly consist of ions having a melting point of less than 100°C. They are also termed as salts which are liquid at room temperature [82]. The first synthesized IL was an ammonium-based one (ethanol ammonium nitrate, EOAN), which was reported by Gabriel in 1888. Ammonium-based ILs have been used widely as electrolytes in high-energy electrochemical devices owing to their good electrochemical cathodic stabilities, low melting points, and low viscosities [83]. ILs have received widespread consideration over the last two decades due to their remarkable properties. These include ease of separation, low or negligible vapor pressure, non-flammability, non-volatility, wide temperature ranges, high thermal stability, mechanical stability, and above all high ionic conductivity [84], [85].

The ionic liquids can be utilized to achieve the desired set of properties for special industrial & consumer applications [86]. Ionic liquids (ILs) have large asymmetric organic cations that are based on 1 alkyl-3-methylimidazolium, N-alkylpyridinium, tetraalkylammonium, or tetraalkylphosphonium cations, and many others. Also, they contain organic or inorganic anions such as hexafluorophosphate $[PF_6]^-$, tetrafluoroborate $[BF_4]^-$, alkylsulfates $[RSO_4]^-$, alkylsulfonates $[RSO_3]^-$, halides as chloride $[Cl]^-$, bromide $[Br]^-$ or iodide $[I]^-$, nitrate $[NO_3]^-$, sulfate $[SO_4]^-$, aluminum chloride $[AlCl_4]^-$, triflate ($[CF_3SO_3]^- = [TfO]^-$) and many others.

Generally, the conductivities of room temperature ILs vary between 1.0 x 10^{-4} to 1.8 x 10^{-2} S/cm. Regardless of broad efforts on high-temperature membranes, so far none of the membranes created meet all the prerequisites for working of PEMFCs at 150°C. When protic ILs are utilized in FCs, the cell can work at temperatures higher than 100^{o}C because the proton transport will be autonomous of the water content inside the cell [34]. In the literature, 1-butyl, 3-methyl imidazolium tri-fluoro-methane

sulfonate was embedded inside the Nafion structure with resulted ionic conductivity of 0.1 S/cm at 180^{o}C [87]. An investigation was performed which indicated that some ILs based on bis(trifluoromethanesulfonyl) amide were electroactive for H_2 oxidation and O_2 reduction under non-humidifying conditions which made them good proton electrolyte membrane competitor in FCs [88].

Ionic liquids can be further classified: protic, aprotic, hydrophilic, hydrophobic, fluorinated, and non-fluorinated. Protic ionic liquids, N-ethyl imidazolium trifluoromethane-sulfonate, have an active portion on large bulky cationic sites which make them highly compatible for use in fuel cells as electrolytes. Under anhydrous conditions, the produced hybrid membranes show proton conductivity up to the order of 10^{-2} S/cm at 160 °C [89]. In comparison to aprotic ionic liquids, protic ionic liquids have high thermal stability and high fluidic properties due to compact arrangements of cationic and anionic active sites [90]. Aprotic are mostly utilized in lithium batteries. Protic ionic liquids are mostly used as electrolytes for fuel cells [88].

Different studies have been reported in the past few years regarding the protic ionic liquids in PEM fuel cells. Lin and coworkers [91] established high-temperature proton exchange membranes for fuel cell operations by functionalizing graphene oxide with protic ionic liquid 1-methylimidazolium trifluoromethanesulfonate and 1-(3-aminopropyl)-3-methylimidazolium bromide. The resulting membranes exhibit good thermal stability and enhanced mechanical properties with a proton conductivity of 1.48×10^{-2} S cm^{-1} at 160°C. The introduction of graphene oxide with ionic liquids enhanced the conductivities of proton exchange membranes in comparison to ordinary membranes [91]. Nakamoto and Noda [92] arranged a protic ionic liquid and organic amines based on bis(trifluoromethanesulfonyl) imide (HTFSI) and benzimidazole (BIm) at different molar proportions The resulting membranes exhibit good thermal stability and enhanced mechanical properties with a proton conductivity of 1.48×10^{-2} S cm^{-1} at 160°C. It had been found that gradually increasing proportions of benzimidazole (BIm) resulted in a good and fast proton transfer. BIm−HTFSI salts were hydrophobic and persisted up to 150 °C for electrode reactions [92][93].

In recent developments, organic or inorganic material can be combined with a variety of ionic liquids to get enhanced physical and chemical properties [94]. The resulting membranes show high thermal stability and mechanical properties at an

optimized cost. Savitha and coworkers designed a new hybrid inorganic-organic proton exchange membranes with a protic ionic liquid triethylammonium trifluoromethanesulfonate incorporated with Nafion and SiO_2. These new hybrid membranes exhibit a conductivity of 4.7×10^{-3} S cm^{-1} at 105 °C [95]. Li & Jiang [96] worked on protic ionic liquid diethylmethylammonium trifluoromethanesulfonate encapsulated with SiO_2 as anhydrous glass membranes. These new hybrid sol-gel process based membranes showed proton conductivity of 10^{-2} S cm^{-1} at 120 – 220°C.

Ionic liquids are the practical option as proton conductors for fuel cell operations. It has been seen that they give high conductivities at high temperatures even without water. Also, the practical applications of ionic liquids fuel cell membranes are limited and further investigations about the real-life operations condition are required. In this thesis, seven ILs were tested in combination to meet the desired objectives and effects on proton conductivities in PEMFCs. For instance, 1-hexyl-3-methyl imidazolium-tri-cyano-methanide has been found to give high conductivities. A new type of proton-conducting hybrid membranes was prepared PIL-based silica hybrid membranes.

2.8.3. Effect of glycerol. Glycerol is an important addition in the enhancement of proton conductivities of membranes due to the presence of three (–OH) groups in its structure which provides extra paths for proton movement as compared to others. Also, glycerol is a well-known plasticizer and cross-linker and one of the additives in fuel cell membrane electrode assemblies [97]. In the past, the effect of glycerol had been reported which contained ZrP/PTFE membrane. The proton conductivities were tested at 200ºC and it was calculated as 0.02–0.045 S/cm approaching to Nafion of 0.1 S/cm [98]. The main reason for the enhancement of conductivities was the increase in proton hopping paths through bulk structure and hydroxyl groups in glycerol.

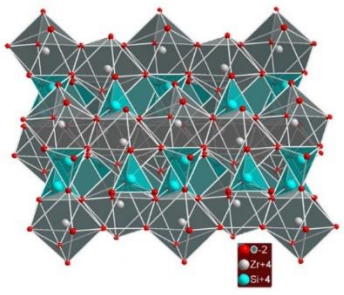

Figure 5: Crystal structure of zirconium silicate (ZrSi) [99]

Chapter 3. Experimental Work

3.1. General Overview

In this chapter, several ionic liquids were incorporated within zirconium silicate ($ZrSiO_4$) materials and were evaluated for their proton-conducting properties. A precipitation reaction was carried out with ionic liquids with $ZrOCl_2$ and Na_2SiO_3 for the synthesis of modified ZrSi/IL materials. A series of characterization tests were performed to study thermal stability, proton-conducting properties, bond nature, and structures with the help of thermogravimetric analysis (TGA), Fourier transform infrared spectroscopy (FTIR), scanning electron microscopy (SEM), X-ray diffraction (XRD) and electrochemical impedance spectroscopy (EIS).

3.2. Material Required

3.2.1. Zirconium oxychloride ($ZrOCl_2$). The $ZrOCl_2$ used in this research was ACS 98% purity and purchased from Sigma-Aldrich

3.2.2. Sodium silicate (Na_2SiO_3). Na_2SiO_3 was ACS 98% purity and purchased from Sigma-Aldrich

3.2.3. Ionic liquids. All ionic liquids were purchased from IoLiTec GmbH. The ionic liquids were used without further purification. Their purity percentages are gives as:

1. 1-Hexyl-3-methylimidazolium tricyanomethanide [HMIM][TCM] > 98%
2. Diethylmethylammonium methanesulfonate [DEMA][OMS] > 98%
3. 1-Butyl-3-methylimidazolium dicyanamide[BMIM][DCA] > 98%
4. 1-Ethyl-3-methylimidazolium methanesulfonate [EMIM][OMS] > 98%
5. Triethylammonium methanesulfonate [TEMA][OMS] > 98%
6. 1-Ethyl-3-methylimidazolium ethyl sulfate [EMIM][ESO4] > 98%
7. 1-Butyl-3-methylimidazolium thiocyanate [BMIM][SCN] > 98%

3.3. Synthesis of Zirconium Silicate/Ionic Liquids Samples

ZrSi/IL samples were prepared by precipitation reaction of $ZrOCl_2$ solution with Na_2SiO_3 in the presence of a series of ionic liquids by the following reaction at room temperature [81]:

$$Na_2SiO_3 + ZrOCl_2 \rightarrow ZrSiO_4 + 2NaCl \quad (14)$$

A solution was prepared by weighing the 0.087g of $ZrOCl_2$ with 0.5 ml of distilled water having a pH of 2.71 and 8 ml of isopropanol. Before the reaction, ionic liquids were added to the $ZrOCl_2$ solution in mass ranging from (0.04 g to 2.735g) which were equivalent to mass percentage of 0.56 % to 32%. Another solution was prepared with 0.033g of Na_2SiO_3 (pH of 10.42) with 8 ml of isopropanol and stirred for 30 minutes. The resulting solution was allowed to react with $ZrOCl_2$ and ILs for 24 hours. After 24 hours, the sample was dried in the oven at ~ 85^oC for 1 to 2 hours.

3.4. Characterization of Zirconium Silicate/Ionic Liquids Samples

Several techniques had been utilized for the characterization of synthesized ZrSi/IL samples as described below:

3.4.1. Electrochemical impedance spectroscopy (EIS) Electrochemical impedance is the response of an electrochemical system (cell) to an applied potential. Fuel cells can be designed as a network of passive electrical circuit elements. A network is called an "equivalent circuit". The EIS response of an equivalent circuit can be calculated and compared to the actual EIS response of the cell.

Electrochemical impedance spectroscopy (EIS) was utilized to determine the proton conductivities in the membranes' sample placing it between two stainless steel electrodes. The response was often non-linear which can be seen in the form of Nyquist or Bode plot from which resistance can be computed. An alternating potential was applied with the help of potentiostat which can be varied up to 0.001 to 7 MHz. The respective resistance (R) value was found from the intersection of the plot with the x-axis at the high-frequency area. Then R-value was utilized in the following equation to calculate the conductivity of the sample [100]:

$$\sigma = \frac{t}{R*A} \tag{15}$$

where, t is the thickness of the membrane sample, A is the cross-sectional area of the cell, and R is the impedance of the sample taken from the EIS plot (Nyquist plot) and reported in S/cm.

3.4.2. High-temperature test. To study the effect of temperature on the proton conductivity of modified ZrSi/IL materials, the best sample were exposed to heat

treatment at 200^{o}C in the oven. After that, the samples were allowed to cool down to room temperature. From that point onward, EIS tests were performed.

3.4.3. Thermogravimetric analysis (TGA). Thermogravimetric analysis (TGA) was used to measure the thermal stability of the material and determine their weight loss as a function of temperature. Water content is a key factor as it is directly related to proton conductivities. TGA analysis was carried out using PerkinElmer, TGA 4000 Thermogravimetric Analyzer. The modified samples were subjected to heat from 27^{o}C to 600^{o}C at a heating rate of 5^{o}C/min, in an inert environment (N_2). TGA curves were discussed for modified materials.

3.4.4. Fourier transform infrared spectroscopy (FTIR). Fourier transform infrared spectroscopy (FTIR) analysis was performed to study the chemical interactions of bonds in modified ZrSi/IL and compare them with bonds of pure ZrSi. It was carried out by using PerkinElmer, Spectrum One FTIR Spectrometer, the wavelength range of 4000 – 450 cm^{-1}.

3.4.5. Scanning electron microscopy (SEM). SEM examination was carried out to study the surface nature (morphology) of the best ZrSi/IL samples. SEM was performed by using Tescan VEGA XMU, LaB6 filament, Oxford Instruments X-Max 50 SSD detector. The SEM images of the synthesized materials were discussed and compared with pure ZrSi.

3.4.6. X-Ray diffraction (XRD). To analyze the crystalline structure of the pure ZrSi and ZrSi/IL samples, XRD analysis was studied. The XRD analysis was done by using Bruker D8 Advance, scintillation point detector, and 1-D detector. ZrSi/IL interactions were discussed by XRD patterns and d-spacing of the best samples.

Chapter 4. Experimental Results & Discussion – Ionic Liquids

Seven ionic liquids were used in this thesis to modify zirconium silicate. Ionic liquids were examined carefully in mass percentages ranging from 0.56% to 32% in this study for their interaction with zirconium silicate. The corresponding highest proton conductivity was reported with an optimized percentage of each ionic liquid. This experimental work also aimed to study the effects of protic versus aprotic ILs and the impact of different cations and anions on the performance of the composite membranes.

The primary objective of this thesis was to develop a Nafion-free ionic liquid-silicate based membranes for high-temperature PEM fuel cell operations. Water content is an important parameter in proton conductivity in PEM fuel cells. So, the ionic liquids types were carefully chosen by acquiring past literature of all hydrophilic nature for enhancements of proton conductivity. Table 3 displays some of the physical properties of the used ionic liquids and their chemical structure can be seen in Figure 6.

Table 3: Physical properties of the tested ionic liquids

Ionic Liquid	Hydrophilic / Hydrophobic	Protic / Aprotic	Viscosity (Pa.s)	Conductivity (S/cm)
[HMIM][TCM]	Hydrophilic	Aprotic	0.0392 [101]	-
[DEMA][OMS]	Hydrophilic	Protic	0.111 [102]	6.2×10^{-3} [102]
[BMIM][DCA]	Hydrophilic	Aprotic	0.0334 [103]	1.052 [104]
[EMIM][OMS]	Hydrophilic	Aprotic	0.135 [105]	3.69×10^{-3} [105]
[TEMA][OMS]	Hydrophilic	Protic	-	1.4×10^{-2} [106]
[EMIM][ESO_4]	Hydrophilic	Aprotic	0.0942 [107]	0.38 [108]
[BMIM][SCN]	Hydrophilic	Aprotic	0.0359 [109]	8.98×10^{-3} [109]

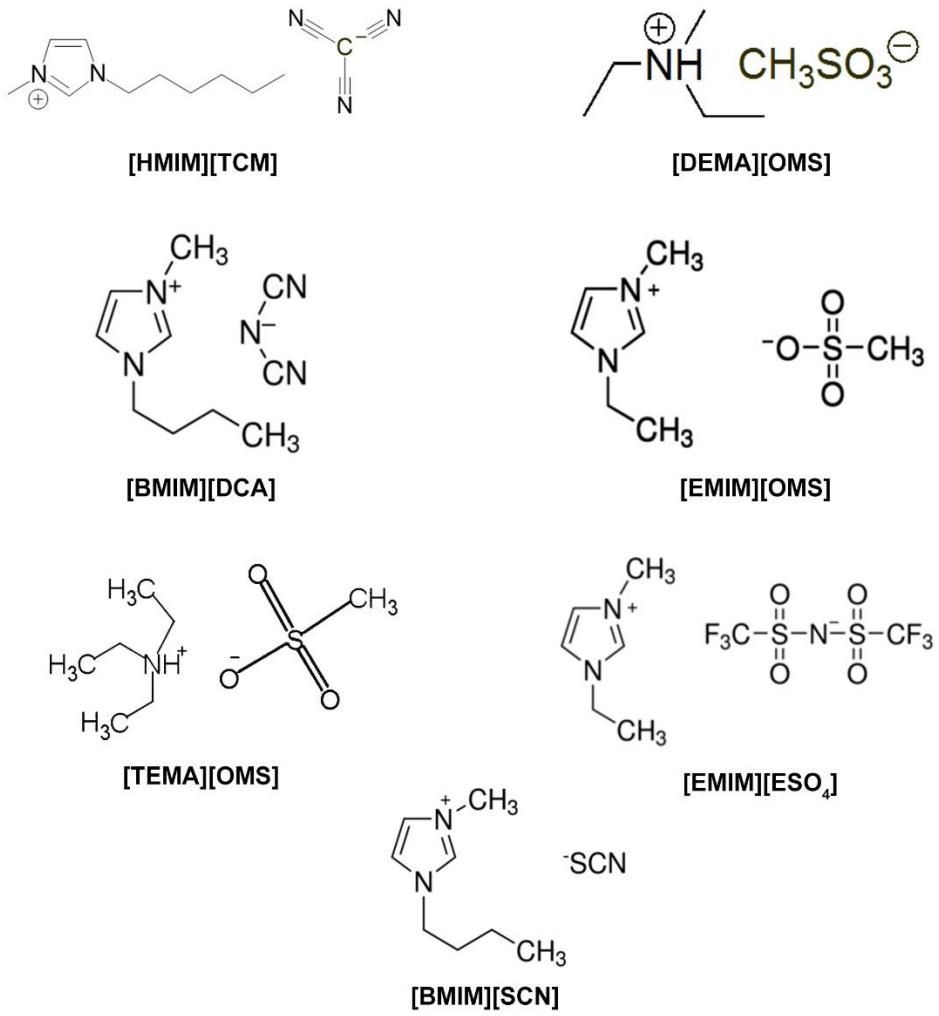

Figure 6: Used ionic liquids chemical structures [101]–[103], [105], [107], [109]

4.1. Conductivity Data

All proton conductivity (S/cm) data related to ZrSi with the incorporation of various seven ionic liquid samples were calculates which also included the best proton-conducting samples. Also, a detailed mass percentage of all ionic liquids is given in the Appendix. Out of seven ionic liquids, two ionic liquids i.e. 1-hexyl-3 methylimidazolium tricyanomethanide ([HMIM][TCM]) & 1-butyl-3 methylimidazolium thiocyanate ([BMIM][SCN]), those having the best conductivity at an optimized amount of ionic liquids have been considered for further analysis. Ramesh [110] and his co-worked reported polymer electrolytes membranes based on thiocyanate and the proton conductivity of value 6.5×10^{-3} S/cm was reported at 343K. Table 4 summarizes the proton conductivity data for different ionic liquids with ZrSi material without any consideration of glycerol.

Table 4: Conductivity data of ZrSi & ZrSi/IL (in this work)

Ionic Liquid	Optimized mass percentages (%) of tested ILs	Conductivity (S/cm)
ZrSi (No IL used)	-	1.45×10^{-3}
ZrSi / [HMIM] [TCM]	21.7 %	7.45×10^{-3}
ZrSi / [DEMA] [OMS]	26.23 %	2.88×10^{-3}
ZrSi / [BMIM][DCA]	1.61 %	1.97×10^{-3}
ZrSi / [EMIM] [OMS]	8.65 %	3.21×10^{-3}
ZrSi / [TEMA] [OMS]	3.75 %	6.97×10^{-4}
ZrSi / [EMIM][ESO_4]	3.23 %	1.37×10^{-3}
ZrSi / [BMIM][SCN]	1 %	2.00×10^{-3}

Electrochemical impedance spectroscopy (EIS) has been examined to determine the proton conductivities for the best ZrSi/IL material whose responses are often linear as well as non-linear which can be seen in the form of a Nyquist plot. Figures 7, 8 & 9 show the EIS plots investigation for pure ZrSi and with two best ZrSi/IL at high-frequency regions.

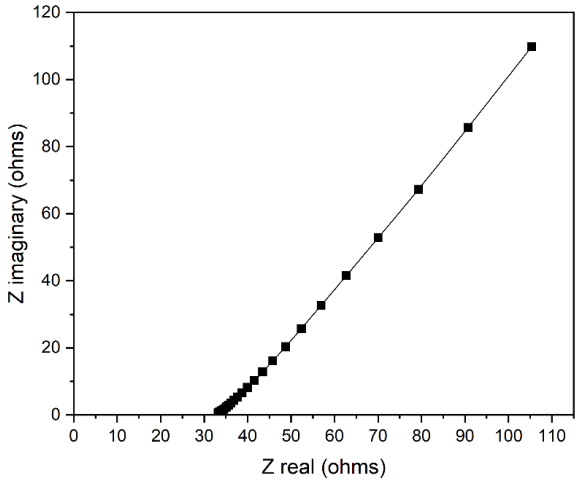

Figure 7: Nyquist plot for pure ZrSi sample with Z = 40.21 ohms

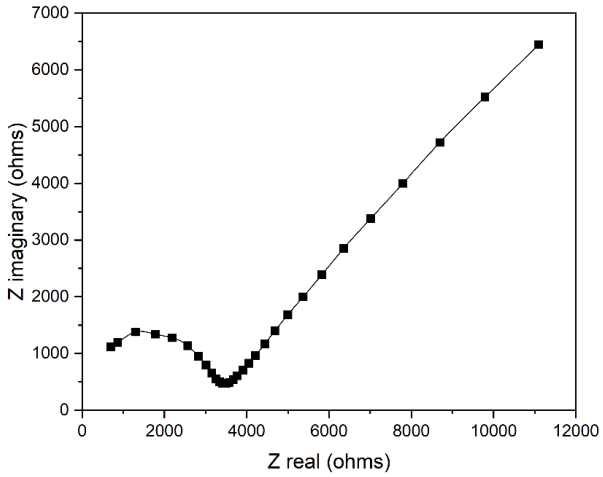

Figure 8: Nyquist plot for pure ZrSi/[HMIM][TCM] with Z = 70.69 ohms

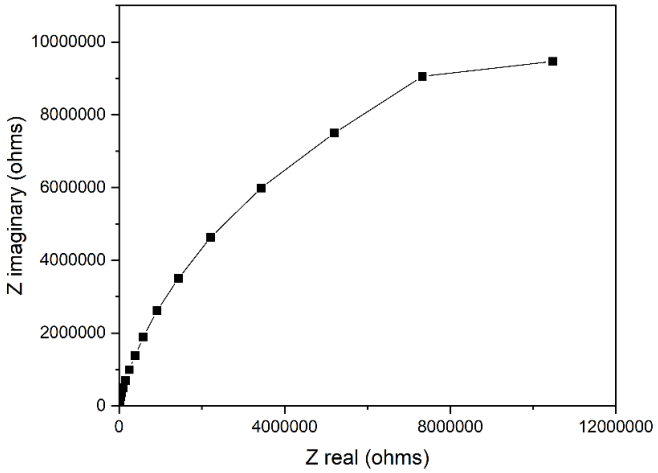

Figure 9: Nyquist plot for pure ZrSi/[BMIM][SCN] with Z = 45.53 ohms

Further, the individual resistance has been computed from the fact of extrapolation of EIS plots at the highest frequency to calculate intercepts with the x-axis. EIS diagrams have been classified based on shapes and mechanisms. EIS diagrams can be a semicircle that depicts a controlled kinetic reaction. Straight lines can be seen in different materials which is an indication of diffusional mechanisms which are also known as the Warburg line. After EIS plots, the resistance for an individual material can be substituted in Eq. (20) from which the proton conductivities can be calculated.

For each ionic liquid used with ZrSi, the proton conductivities increase with increasing mass percentages (%) up to optimized amounts which were succeeded by certain trends. Figures 10 and Figure 11 display different values of proton conductivities as a function of the mass percentage of ionic liquids. Figure 10 shows a slightly decreasing trend for the first percentages of IL addition. After 15.52% mass

addition, the trend shows a sharp increase which displays a value of 7.45 x 10^{-3} at 21.7% mass addition. Figure 11 demonstrates that ZrSi/1-Butyl-3-methylimidazolium thiocyanate reaches a maximum of 2.00 x 10^{-3} S/cm at a mass percent of 1% and after that, an increment in mass percentage leads to a decrease in overall proton conductivity. An addition of ionic liquid intercalates the ZrSi crystal structure which is responsible for the peculiar behavior of conductivities. Further, maximum proton conductivity measurements are available for different ionic liquids with their mass percentages.

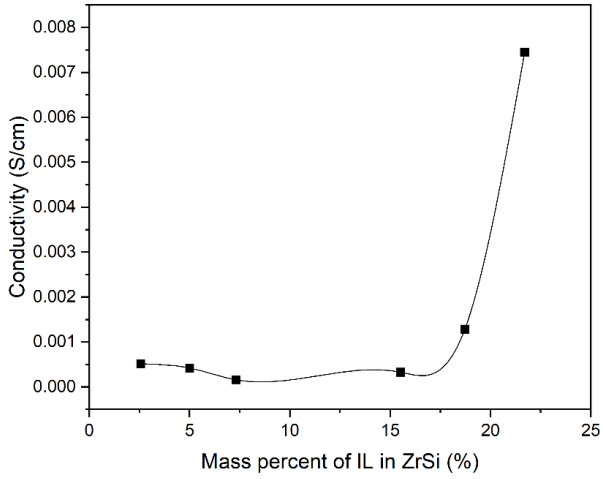

Figure 10: Mass percentage vs conductivity for ZrSi/[HMIM][TCM]

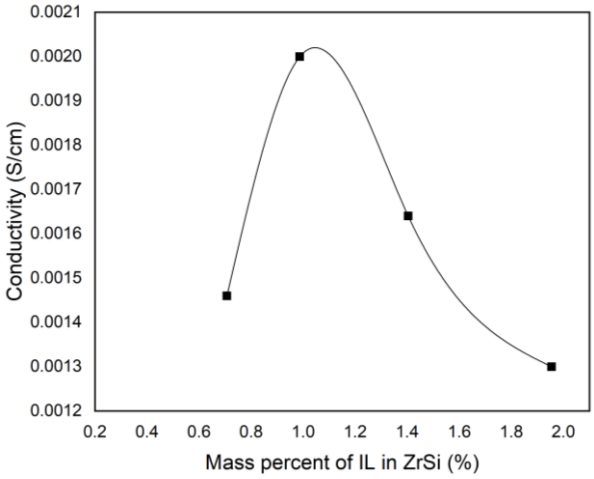

Figure 11: Mass percentage vs conductivity for ZrSi/[BMIM][SCN]

A detailed investigation for proton conductivity behaviors of various ionic liquids can be done by examining the chemical structures as shown in Figure 6. The conductivity values are listed in Table 4.

So far two aprotic ionic liquids have been considered for further analysis which involves no mass percentages of glycerol. Both ionic liquids are hydrophilic and the

maximum proton was come out to be 7.45 x 10^{-3} & 2.00 x 10^{-3} S/cm with [HMIM][TCM] and [BMIM][SCN] respectively.

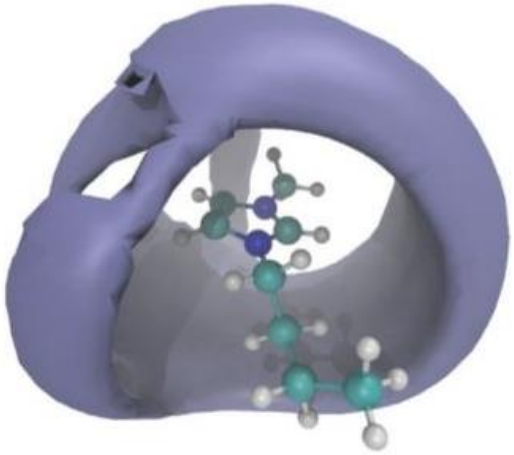

Figure 12: Function of central carbon in [TCM] anion of imidazolium ring [111]

The proton conductivity can be explained based on hydrogen bonding. In literature, hydration dynamics of [HMIM][TCM] (Figure 12) were studied which showed that water molecules were hydrogen-bonded with $[TCM]^-$ ions through bending of C−C−N in nitrile groups and carbon atoms rings [112]. So, the hydrogen bonding between [HMIM][TCM]/ZrSi is anticipated that causes more hopping space for proton movements. Also, the structural arrangement of the anionic part $[TCM]^-$ can increase the formation of more hydrogen bonds which lead to more paths for proton movements. Moreover, TGA and water uptake analysis showed its thermal stability up to 500^{o}C with minimum weight losses. These are some reasons which might explain the highest conductivity in the case of [HMIM][TCM].

[BMIM][SCN] also showed good proton conductivity values but it has lower than ZrSi/[HMIM][TCM]. The decrease in conductivity values can be explained based on intermolecular interactions in the bulk of ionic liquids. An increase in ion size can increase the viscosity of liquids and hence the energy of cohesion is also increased which ultimately reduces the electrostatic attractions [113]. [BMIM][SCN] is also hydrophilic but weak hydrogen bonding with ZrSi structures is expected. Although, $[SCN]^-$ shows less attraction towards water molecules which may lead to low proton conductivity values but TGA showed its thermal stability up to 500^{o}C.

Chapter 5. Experimental Results & Discussion – Effect of Glycerol

Glycerol was considered as an additive due to its remarkable characteristics as a dispersing agent, cross-linking, and proton conductivity. In this thesis, a detailed investigation was carried out to investigate the proton conductivity of various combinations of ZrSi/GLY/IL membranes for PEM fuel cell operation.

An experimental procedure was followed for the addition of glycerol amounts to $ZrOCl_2$ solutions and ionic liquids combinations. Glycerol amounts were added carefully in the ranges of 0.15% to 2.58% to $ZrOCl_2$ & IL suspensions which was preceded by the typical precipitation reaction of Na_2SiO_3 for preparation of newly modified membranes based on ZrSi/GLY/IL. Then, characterization tests were done which include EIS, FTIR, XRD, EDX, TGA, and SEM. The physical characteristics of glycerol have been mentioned in Table 5. Also, the chemical structure of glycerol is displayed in Figure 13. As glycerol, a non-volatile compound, contained strong hydrogen bonds in its structure which leads to high boiling point (290^oC). Also, the proton conductivity value (3.28 x 10^{-3} S/cm) of pure glycerol was reported in this thesis.

Table 5: Physical properties of Glycerol [115]

Properties	Literature values
Density	1260 kg/m^3
Viscosity (^oC)	1400 mPa.s
Melting point	18 ^oC
Boling point	290 ^oC
Surface tension	63.4 mNm^{-1}

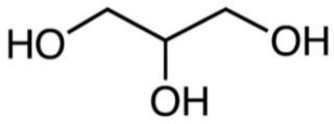

Figure 13: Chemical structure of Glycerol [114]

5.1. Conductivity Data

Electrochemical impedance spectroscopy (EIS) were applied to perform proton conductivity analysis based on Nyquist Plots for the two best modified ZrSi/GLY/IL membranes for PEM fuel cells. The plots for different samples are displayed in Figure 14 and Figure 15. The resistance values were computed by extrapolation mathematical technique to obtain intercept with the x-axis at the high-frequency region. Then equation (15) was applied to get the proton conductivity for individual samples.

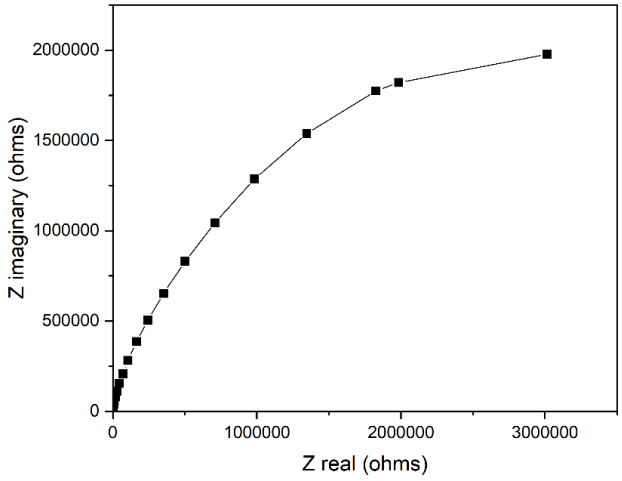

Figure 14: Nyquist plot for pure ZrSi/[HMIM][TCM]/GLY with Z = 0.458 ohms

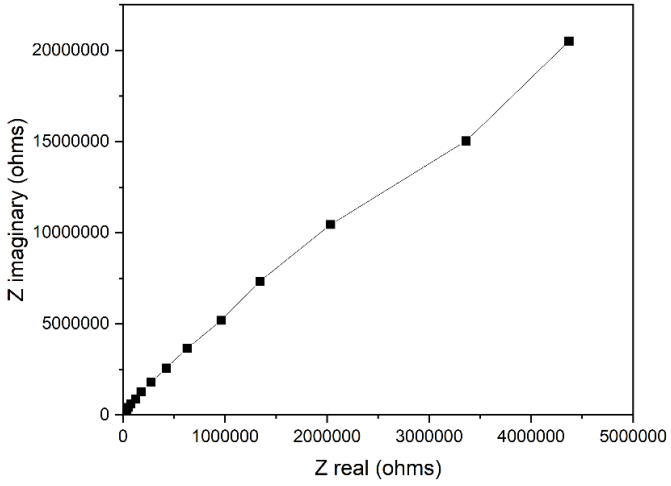

Figure 15: Nyquist plot for pure ZrSi/[BMIM][SCN]/GLY with Z = 0.892 ohms

Table 6 shows the conductivity values of two best modified samples with respect to values obtained from EIS plots. Figure 16 displays the trends for mass percentage vs conductivity for three different ZrSi/IL materials to glycerol addition. The conductivity value increased from 10^{-3} S/cm to 10^{-1} S/cm with the addition of

glycerol. It reaches at a maximum values of 0.196 S/cm and 0.1 S/cm with 0.469% and 0.387% by mass glycerol for ZrSi/[HMIM][TCM] & ZrSi/[BMIM][SCN] respectively. After that, the conductivity trends go downward with other variations in glycerol amounts. A maximum amount of glycerol and ionic liquids can intercalate between the layers of ZrSi that forms multiple hydrogen bonds. Hence, limiting reactants between glycerol and ionic liquids can cause decrease in proton conductivities.

Table 6: Conductivity data of ZrSi/IL/GLY

ZrSi/Ionic liquid	Optimized mass (%) of Glycerol	Conductivity (S/cm)
ZrSi/[HMIM][TCM]	0.469 %	0.196
ZrSi/[BMIM][SCN]	0.387 %	0.1

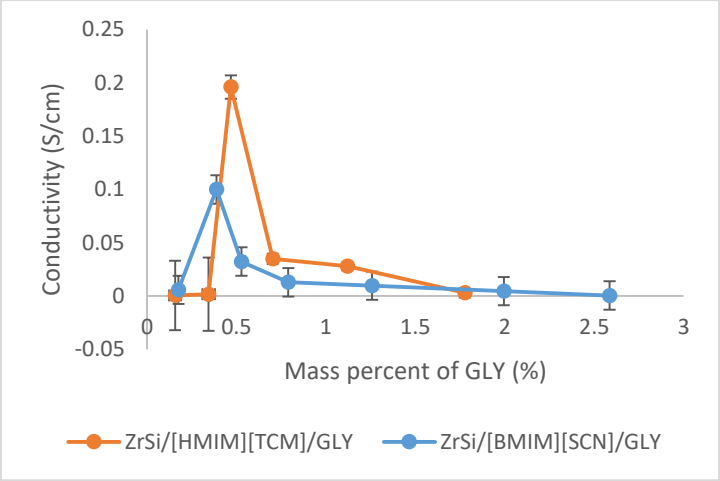

Figure 16: Mass percentage vs conductivity for ZrSi/IL/GLY modified samples

The addition of glycerol (GLY) has tremendously improved the proton conductivities of ZrSi/IL material. It is anticipated that the intercalation of glycerol in ZrSi layer has enhanced the conductivity and a certain amount of glycerol can be adjusted between the layers. The chemical structure of glycerol can explain the increase in proton conductivity. Figure 13 depicts the chemical structure which has three hydroxyl groups (-OH). Hence, its incorporation with ZrSi/IL can provide more paths for proton hopping which increases proton conductivities.

5.2. Thermogravimetric Analysis (TGA)

The thermal stability and water loss (%) of the best modified ZrSi/IL materials were studied by performing the thermogravimetric analysis (TGA) and compared with pure ZrSi. The modified samples were subjected to heat from 27ºC to 600ºC at a heating rate of 5ºC/min in an inert environment (N_2). Also, TGA was examined on the samples that showed the highest values of conductivities. Figures 17 displays the TGA analysis of pure ZrSi and the modified ZrSi/IL samples.

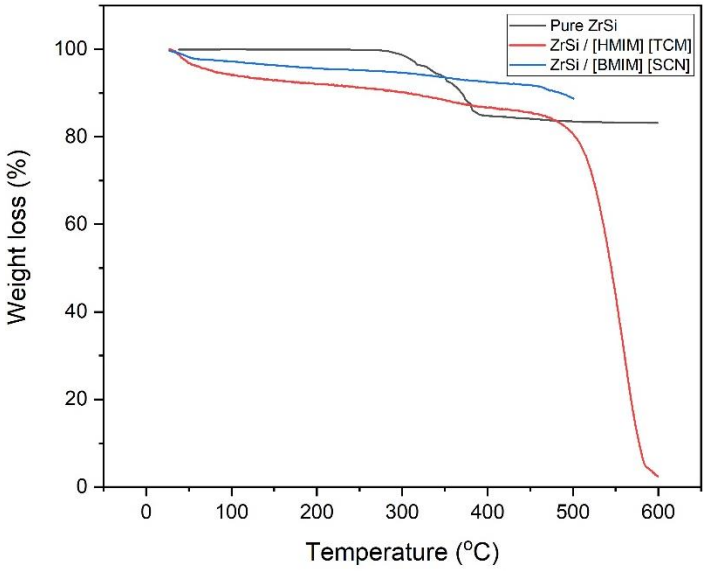

Figure 17: TGA analysis for ZrSi and ZrSi/IL samples

In Figure 17, TGA analysis for pure ZrSi sample showed a 3% weight loss up to 320°C which was an attribution of oxidative decomposition of lattice and loss of water molecules due to Si–O–H condensation [80] and it was followed by a maximum loss at 600°C. TGA analysis of the modified ZrSi/[HMIM][TCM] material demonstrated a steadily 18% weight loss at around 490°C which was followed by a sharp decrease up to 600°C. ZrSi/[BMIM][SCN] displayed a 10% weight loss which was seen at around 500°C. Excellent TGA curves indicate good thermal stability at higher temperatures. Overall, it was seen that ZrSi/[BMIM][SCN] showed excellent thermal stability in comparison with ZrSi/[HMIM][TCM] which was due to more water uptake properties.

Overall, it has been examined that modified ZrSi samples with different ionic liquids have enhanced the water content abilities. It can be seen from TGA curves that

modified samples have excellent water take-up properties with a very small weight loss in the temperature range up to 200°C in comparison with pure ZrSi with no ionic liquid which is in agreement with the proton conductivities results. Also, modified materials formed multiple hydrogen bonds with ionic liquids and glycerol. Hence, ZrSi/[HMIM][TCM] & ZrSi/[BMIM][SCN] showed excellent thermal stability with minimum weight loss which can work at high-temperature fuel cell applications.

5.3. Fourier Transform Infrared Spectroscopy (FTIR)

FTIR analysis was carried out to study the chemical bond interactions in pure ZrSi and the modified ZrSi/IL samples. FTIR was also performed on the best samples with the highest proton conductivity values. The FTIR spectrum for pure ZrSi and modified ZrSi/IL samples are displayed in Figures 18 and Figure 19 respectively. In Figure 18, the FTIR spectra for pure ZrSi showed a shoulder around 1077-1170 cm^{-1} which depicted the strongest region of all silicates exhibiting an internal symmetric stretching between Si-O-Si of SiO_4 structures [115]. The embodiment of hetero-atom and vibrational stretching were demonstrated by the region of 960-980 cm^{-1}. Incorporation of zirconium (Zr) into lattice structure can be found at lower wavenumbers [116]. All samples consisted of certain entrapped water molecules in the structures. Furthermore, sharp peaks were observed at 1640-1835 cm^{-1}. These peaks are attributions of H-O-H stretching of entrapped water molecules [117]. A band at 2750-3750 cm^{-1} are characteristics of asymmetric stretching vibration of silanol OH groups (Si–O–H) [118].

In Figure 19, FTIR spectra for the best samples i.e. ZrSi/[HMIM][TCM] and ZrSi/[HMIM][SCN] are displayed. Both spectra for the modified samples followed the same trends. A shoulder at around 1170-1185 cm^{-1} demonstrated symmetric stretching between Si-O-Si. Also, the characteristic strong band at 1625 cm^{-1} exhibited the bending vibrations modes of aromatic ring C=C and C=N bond [119]. A stronger C-C stretching was observed in the ZrSi/[HMIM][TCM]. The modified samples showed a peak at 2370 cm^{-1} which was an attribute of asymmetrical stretching of C-N bonds [120]. Cyanate (-SCN) stretching occurred at around 2240 cm^{-1}. The symmetrical vibrational stretching of C-H alkyl showed absorption bands of 2870-2970 cm^{-1}[121]. Water molecules vibration displayed at around 3370 cm^{-1} [122]. Overall, FTIR spectra for pure ZrSi and ZrSi/IL were quite similar. The intensity of peaks of O-H peaks was

higher for all modified material in comparison with pure ZrSi. Hence, it is anticipated that modified samples contained a certain amount of water content in their lattice structures [118]. Also, TGA analysis showed higher water uptakes in ZrSi/IL than pure ZrSi. Moreover, the bands around 1320-1480 cm^{-1} showed intercalation of ionic liquid in ZrSi structures.

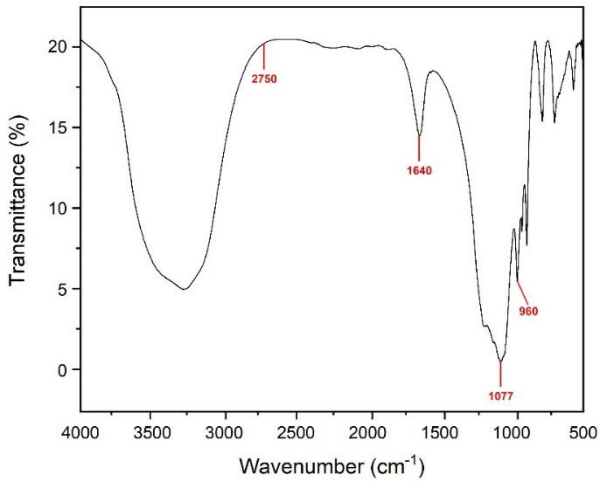

Figure 18: FTIR spectra for pure ZrSi

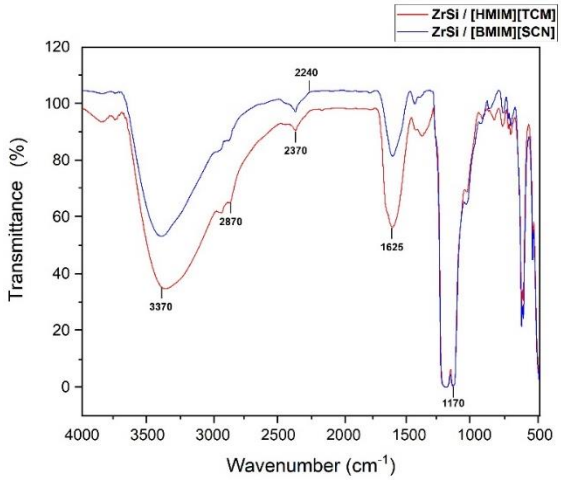

Figure 19: FTIR spectra for modified ZrSi/IL samples

5.4. Scanning Electron Microscopy (SEM)

Scanning electron microscopy was performed to examine the surface morphology of pure ZrSi and modified ZrSi/IL materials. SEM images are given in Figures 20, 21, and 22. Figure 20 portraits a top view image of surface morphology of pure ZrSi. The particles followed a cubic structure with some tetrahedron like shapes

which was also compared with crystallography open database [123].

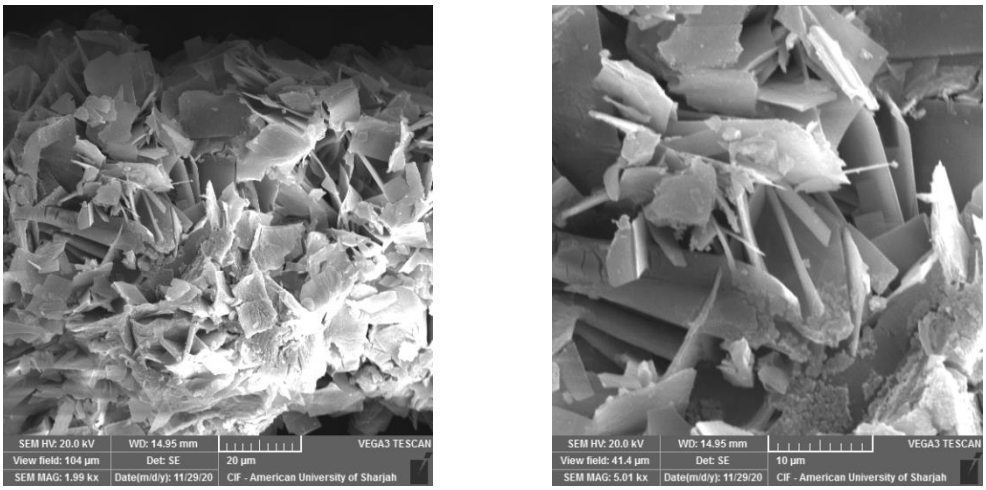

(a) (b)

Figure 20: SEM images for pure ZrSi at magnification of (a) 2000X (b) 5000X

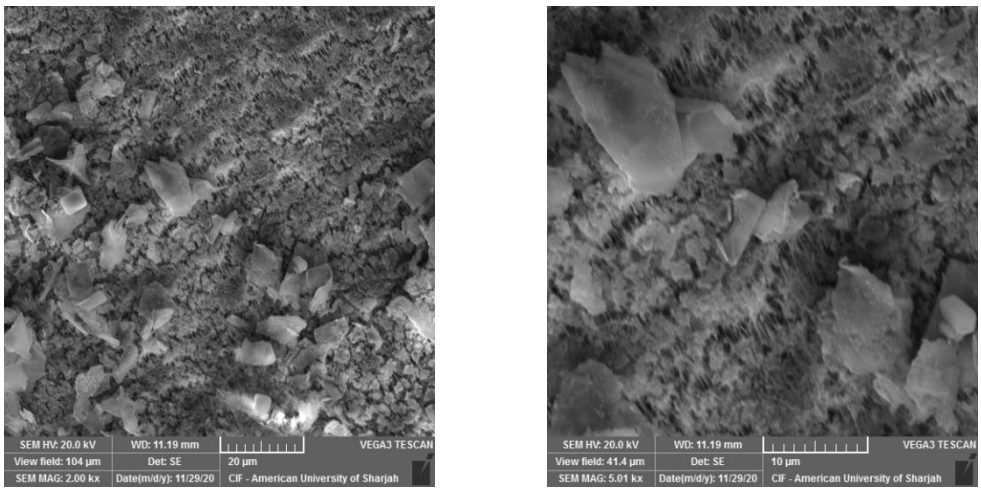

(c) (d)

Figure 21: SEM images for ZrSi/[HMIM][TCM] at magnification of (c) 2000X (d) 5000X

Overall, it was observed that the particle diameters decreased on the addition of ionic liquids which enhanced the available surface areas of the structure. Also, it can be anticipated that ionic liquids have promoted the nucleation among the layer of ZrSi structure which leads to modification in crystalline structures in comparison with pure ZrSi. Figure 21 and Figure 22 display SEM images for the best two modified samples i.e. ZrSi/[HMIM][TCM] & ZrSi/[BMIM][SCN] respectively. In the case of

ZrSi/[HMIM][TCM], the particles looked like orthorhombic cubical structure. Monoclinic structures were seen on SEM analysis for ZrSi/[BMIM][SCN].

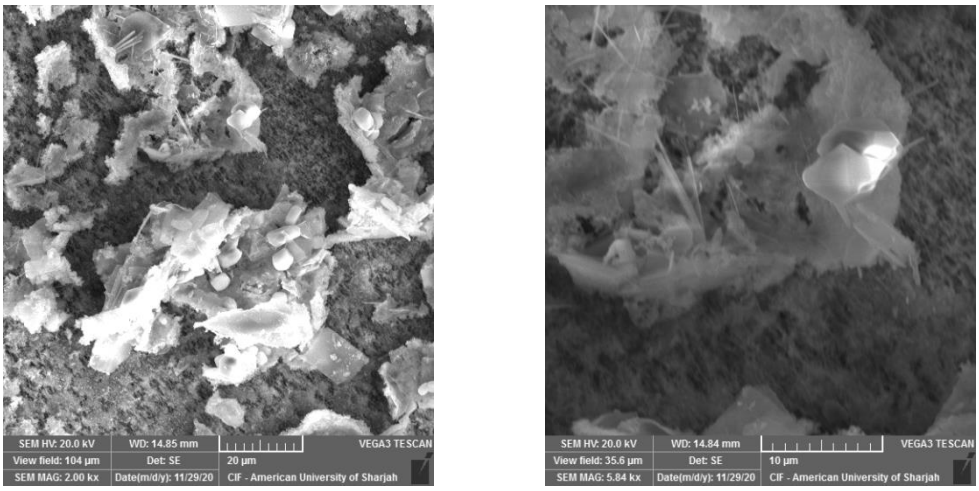

(e) (f)

Figure 22: SEM images for ZrSi/[BMIM][SCN] at magnification of (e) 2000X (f) 5800X

5.5. Energy Dispersive X-ray (EDX)

For the quantitative elemental study, EDX was carried out in conjunction with SEM for different samples. EDX was studied in different areas of pure ZrSi and modified material. The abscissa of the EDX spectrum displays the ionization energy and ordinate indicates the counts. The corresponding peaks are shown in Figures 23, 24 and 25.

In the pure ZrSi spectrum, the atomic ratios of elements (O:Si:Zr:Cl) were calculated as 0.694, 0.272, 0.023, and 0.001. This ratio depicts that oxygen and silicon contents were higher than that of Zr and Cl in the pure sample. On the addition of ionic liquid & glycerol, it is anticipated the changes in zirconium silicate structures. The spectrum of ZrSi/[HMIM][TCM] displayed the values of atomic ratios as 0.708, 0.219, 0.036, 0.035 respectively, while in the spectrum of ZrSi/[BMIM][SCN], the observed atomic ratios for O, Si, Zr & Cl were 0.68, 0.28, 0.027, and 0.008 respectively.

Overall, it can be seen from oxygen content for ZrSi/[HMIM][TCM] is higher than ZrSi/[BMIM][SCN] which depicts an increase in hydrogen bonding in structures. Hence, it is expected that it will have high proton conductivity values.

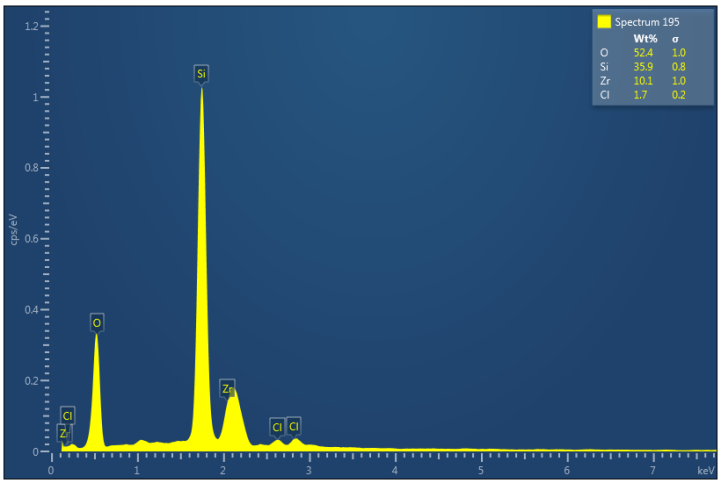

Figure 23: EDX for pure ZrSi sample

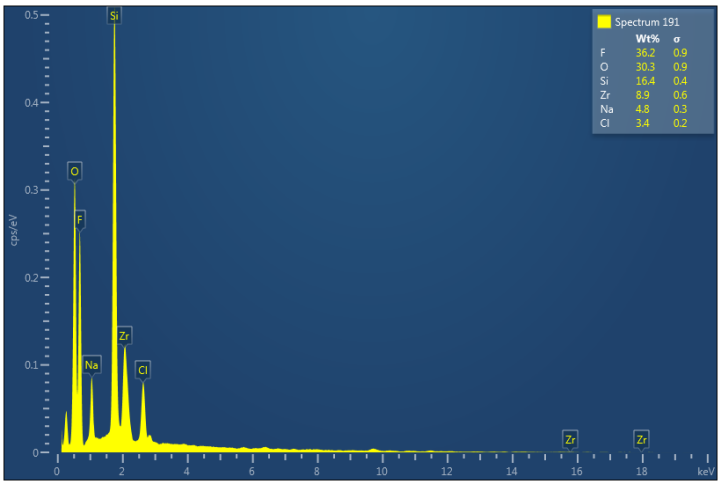

Figure 24: EDX for ZrSi/[HMIM][TCM]

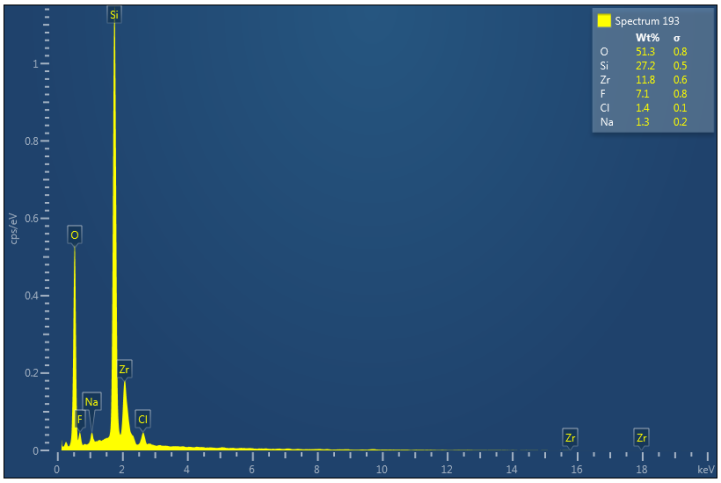

Figure 25: EDX for ZrSi/[BMIM][SCN]

5.6. X-ray diffraction (XRD)

For the investigation of crystal structures of the modified samples, XRD analysis was performed. XRD patterns for pure ZrSi and modified samples are given in Figure 26 and Figure 27.

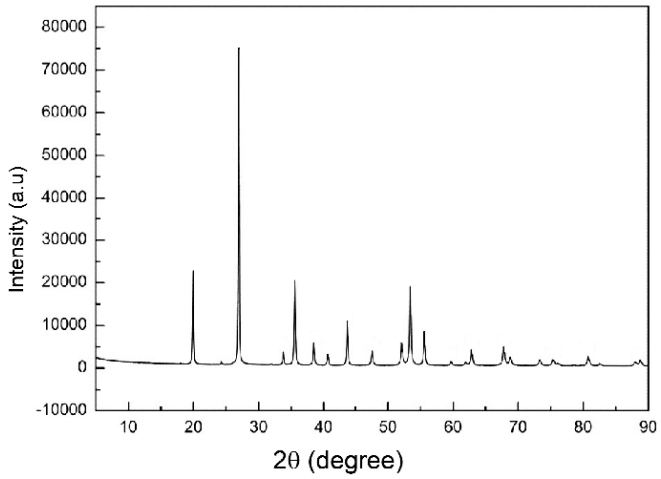

Figure 26: XRD pattern of zirconium silicate ($ZrSiO_4$) [124]

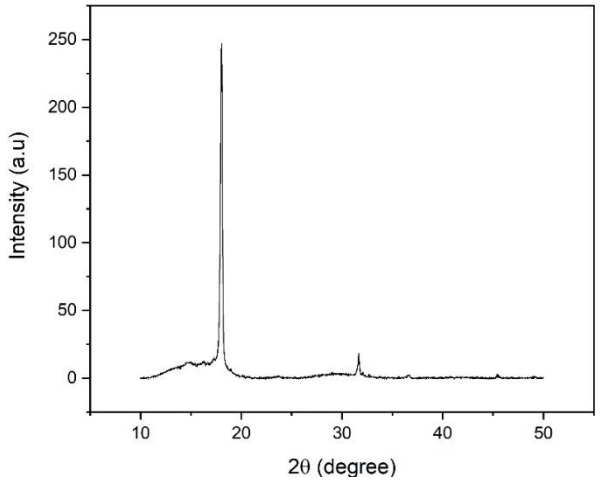

Figure 27: XRD pattern of ZrSi/[BMIM][SCN]

Overall, it is seen that samples have narrow peaks with a sharp intensity which leads to the conclusion that those modified materials possess crystalline structures. The crystalline structure of ZrSi permits the water molecules to be intercalated with its layers at the surface [125]. As crystallinity increases then surface water will decrease [126]. Also, the XRD pattern demonstrates different peak intensities at different 2θ (degree). Deflection of beams can be obtained from θ values. Bragg's law [127] can be applied for the calculations of d-spacing values between atoms of the modified samples.

Pure ZrSi shows sharp peaks at 2θ of about 20.09°, 27.08°, 35.69°, and 53.54°. These deflection values were compared with the available literature review [124]. For ZrSi/[BMIM][SCN] sample, the values of 2θ can be seen around 18.05°, 31.65°, 36.65° and 45.42°. Pure ZrSi has polymorphic crystallographic structures that depict that beyond critical particle diameter, a monoclinic transformation occurred [128]. A comparison between pure ZrSi and ZrSi/IL shows that the peaks on 20° and 27° have disappeared which shows major changes in the crystal structures. This indicates the intercalation of ionic liquids into ZrSi layers which change the distance between the layers. Using Bragg's law, d-spacing values at different deflections can be obtained from equation (22) [127]:

$$2\,d\sin\theta = \lambda \tag{22}$$

5.7. Conductivity at High-Temperature

One of the primary objectives of this comprehensive study was to examine the proton conduction at high temperatures i.e. 200°C. To accomplish this, the modified ZrSi/IL/GLY was subjected to heat analysis in an oven at 200°C for 30 to 40 minutes. After that, the samples were cooled down at ambient temperature and then the proton conductivity of samples was determined using EIS plot as displayed in Figure 28 ([HMIM][TCM]) and Figure 29 ([BMIM][SCN]). Table 7 shows the high-temperature conductivity test results at 200°C.

Table 7: High-temperature conductivity test for ZrSi/IL/GLY at 200°C

Sample (ZrSi/IL/GLY)	Conductivity (S/cm)
ZrSi / [HMIM] [TCM]	2.40×10^{-3}
ZrSi / [BMIM][SCN]	2.90×10^{-3}

With the increase in temperature, the conductivity declined by two orders of magnitude. The main reason behind the decrease in conductivity is the evaporation of water content present on the membranes. Following TGA, the modified materials were still mechanically and thermally stable due to modification of internal structural arrangement and high decomposition temperature of ZrSi/IL/GLY. After a high-temperature test, the results and performances are still more promising in comparison

to ordinary Nafion. With the relative humidity of 34%, Nafion has a conductivity 1.40 x 10^{-4} S cm^{-1} at 30ºC [129]. In this work, the conductivities were reported in order of 10^{-3} S cm^{-1} at 200ºC.

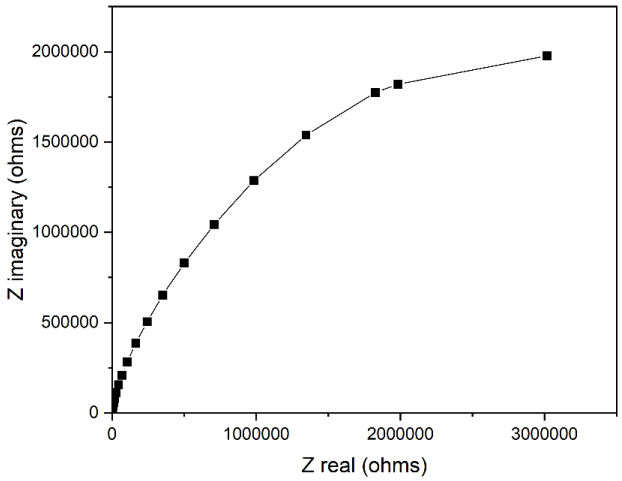

Figure 28: Nyquist plot (high-temperature test) of best samples at Z = 37.35 ohms

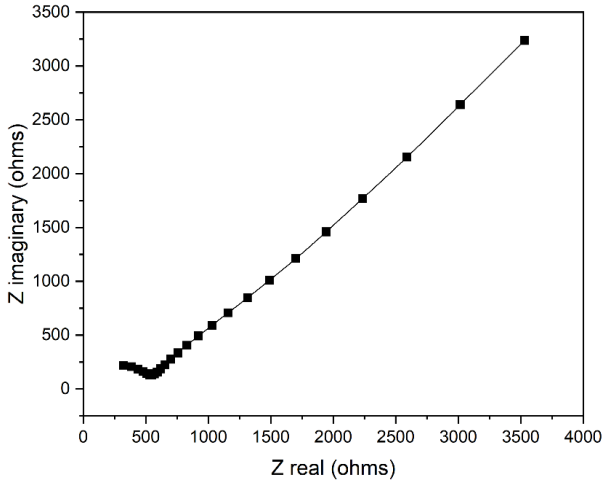

Figure 29: Nyquist plot (high-temperature test) of best samples at Z = 30.91 ohms

5.8. Water Uptake Analysis

An optimum amount of water is required for proton hopping which leads to good proton conductivity. This analysis shows the relative amounts of water contents on the membranes before and after the application of heat. To accomplish this, the modified ZrSi/IL/GLY was subjected to water take up analysis with the immersion of the sample into the water. Then, the samples were dried in an oven at 80°C. The weights of membranes of both dry and wet were determined. A comparison of water take-up percentages (%) of the best samples and other composite membranes with pure ZrSi

are given in Table 8. Water content is an important factor in determining the proton conductivity. Pure ZrSi sample contained a water uptake percentage of 19.23%. The modified material ZrSi/[HMIM][TCM] and ZrSi/[BMIM][SCN] materials showed a water content of more than 50%. This value was compared with Nafion composite membranes and appeared to be promising. Hence, with this reasonable water uptake, it is anticipated that new modified materials can perform well at high-temperature operation.

Table 8: Comparison of water uptake analysis for ZrSi/IL/GLY

Samples	Water take-up percentages (%)
ZrSi (No IL used)	19.23 %
ZrSi/[HMIM][TCM]	53.51 %
ZrSi/[BMIM][SCN]	57.89 %
Nafion-Zeolite 10 [130]	43.7 %
Nafion/TiO_2 [131]	51 %

5.9. Discussions

Overall, the results showed that the addition of ionic liquids to the ZrSi material enhanced their proton conductivity. Seven ionic liquids were investigated and the modified composite materials were evaluated for their proton-conducting properties. The ionic liquids were added at different mass percentages ranging from 0.56% to 32% (without glycerol) as shown in Table 4. The results showed an enhancement in proton conductivity as opposed to the unmodified ZrSi/PTFE membranes. The increase in conductivity could be attributed to several factors.

First, the hydrophilicity of the ionic liquids utilized in this thesis as they are expected to retain more water molecules inside ZrSi materials. , The highest conductive samples based on the two ionic liquids i.e. 1-hexyl-3-methylimidazolium tricyanomethanide ([HMIM][TCM]) and 1-butyl-3-methylimidazolium thiocyanate ([BMIM][SCN]), were considered for further analysis.

Second, there is a strong relationship between viscosity and proton conductivities as ionic liquids with low viscosities have excellent proton conductivities [132]. In the case of [HMIM][TCM], an increase in alkyl chains of cationic imidazolium part will provide a resistance to flow which are mainly due to increased interactions and large sizes of alkyl chains [111]. Hence, it leads to low diffusivity and ions will require more energy to overcome the energy barrier. Consequently, proton conductivities will decrease. Table 3 shows the viscosities for different ionic liquids at room temperatures. So, the incorporation of ZrSi will modify the proton conductivities with different percentages of ionic liquids as shown in Table 4.

Ionic liquids are liquid salts that are typically formed by passive movements of protons from Bronsted acids to Bronsted bases [96]. One way to explain the ionicity of ionic liquids, viscosity, and their effect on proton conductivity is the Walden rule which stated that ionic conductivity can be explained as the product of the inverse of viscosity and summation of the reciprocal distance of cationic and anionic parts of ionic liquids [133]. Walden plot [134] also showed that the conductivities of ionic liquids are inversely related to viscosities. The main reason for the increase of conductivities in the case of 1-hexyl-3-methylimidazolium tricyanomethanide ([HMIM][TCM]) & 1-butyl-3-methylimidazolium thiocyanate ([BMIM][SCN]) was followed by the Walden rule. [HMIM][TCM] has low viscosity in comparison with [BMIM][SCN]. Out of two ZrSi/IL materials, 1-hexyl-3-methylimidazolium tricyanomethanide ([HMIM][TCM]) with ZrSi has the highest proton conductivity value of 7.45×10^{-3} S/cm.

The second phase of the experimental study was to study the effects of glycerol amounts on modified ZrsI/IL material. Table 6 shows conductivity data concerning glycerol amounts (%). It was verified that the addition of glycerol had enhanced the proton conductivity for ZrSi/IL materials. For instance, 1-hexyl-3-methylimidazolium tricyanomethanide ([HMIM][TCM]) has high proton conductivity of 0.196 S/cm with 0.469% of glycerol. In the case of 1-butyl-3-methylimidazolium thiocyanate ([BMIM][SCN]), a high proton conductivity of 0.1 S/cm can be seen with 0.387% of glycerol amounts. Another reason for the sharp increase in conductivities of ZrSi/IL was the addition of glycerol as glycerol structures contained three hydroxyl groups (-OH) which provided more paths for proton hopping [98]. Also, glycerol behaved as a cross-linker that forms multiple hydrogen bonds in ZrSi structures. FTIR analysis of

[HMIM][TCM] showed strong C-C and water absorption bands which depicted a strong interaction between glycerol, alkyl group, and water.

Different characterization techniques were applied to the best-modified samples to discuss their thermal and chemical properties. TGA analysis for ZrSi/IL/GLY was done to examine the thermal stability of the sample at high temperatures. TGA analysis showed a weight loss of 10-20% at around 500^{o}C with a maximum loss at 600^{o}C. The addition of glycerol also enhanced water take-up properties. Table 8 shows the remarkable water uptake of the modified ZrSi/IL/GLY samples in comparison with pure ZrSi. The results are consistent with the proton conductivity data for the modified samples.

Surface morphology & elemental composition analysis were discussed by using SEM and EDX. SEM images showed crystalline structures of ZrSi/IL/GLY samples. Nucleation among the layer of ZrSi structure was enhanced with the decrease in particle diameters which exhibited modification in crystalline structures in comparison with pure ZrSi. All modified samples belonged to cubic crystallography which was further examined in orthorhombic and monoclinic crystalline structures for the two best samples. Also, EDX analysis shows an increase in hydrogen bonding modified samples which showed enhanced proton conductivities of samples.

For further investigation of crystalline structures, FTIR and XRD were performed on different samples that displayed intercalations of ionic liquid in ZrSi structures which were proof that modified materials also contained a well-defined class of crystalline structures. The high-temperature (200^{o}C) analysis also showed the mechanical and thermal stability of modified materials as ZrSi/IL/GLY can sustain more than 200^{o}C due to intermolecular forces of attraction. A decrease in proton conductivity of modified samples which were mainly due to water evaporation losses at high-temperature but still, showing promising conductivities in comparison with Nafion. Throughout the work, the proton conductivities of 0.1-0.2 S/cm were achieved which exceeded that of ordinary Nafion (0.1 S/cm).

Chapter 6. Conclusions and Future Work

6.1. Conclusions

The scope of this comprehensive study was to develop Nafion-free proton conducting membranes based on zirconium silicates (ZrSi) & ionic liquids. Modified proton conducting materials based on ZrSi/IL/GLY were synthesized and characterized by techniques of TGA, FTIR, XRD, SEM, and EDX. The modified materials were synthesized with the help of different ionic liquids and $ZrOCl_2$ which are followed by a precipitation reaction of Na_2SiO_3. Seven ionic liquids were examined which included: [HMIM][TCM], [DEMA][OMS], [BMIM][DCA], [EMIM][OMS], [TEMA][OMS], [EMIM][ESO_4], and [BMIM][SCN].

The proton conductivity of the pure sample (ZrSi) was 1.45 x 10^{-3} S/cm. Out of seven ionic liquids, the proton conductivities of the best-modified samples were reported as 0.196 and 0.1 S/cm, obtained from two ionic liquids [HMIM][TCM] and [BMIM][SCN], approaching Nafion (0.1 S/cm).

In general, the addition of ionic liquids increased the proton conductivity of ZrSi by two orders of magnitude. The incorporation of ionic liquids between the ZrSi structures enhanced the proton hopping. The hydrophilicity of ionic liquids played an important part in the increase in proton conductivity. The addition of glycerol also provided more paths for proton movements which ultimately increased the conductivity of samples. All these results were verified by different characterization.

The modified ZrSi/IL material was tested at a high temperature of 200^{o}C. With an increase in temperature, the proton conductivities were decreased drastically but the results were still better than ordinary Nafion membranes, which was due to loss of water content while Nafion showed a decrease in its conductivity when it was operated at above 100^{o}C.

The study of water uptake analysis and proton conductivities with the incorporation of ZrSi/IL with optimized amounts of glycerol showed better results than ordinary Nafion. Hence, it can be anticipated that modified ZrSi/IL materials with glycerol amounts can be an alternative to ordinary membranes for high-temperature PEM fuel cell operations.

6.2. Future Work Recommendations

1) Prepare zirconium silicate (ZrSi) with other chemical methods and study the effects of thermal stability and proton conductivities.
2) Synthesize membranes with the other ionic liquids having similar anions for understanding the different types of ionic liquids and testing their proton conductivities.
3) Characterization & mechanical study of high temperature processed membrane.
4) Synthesize proton conducting membranes based on SPEEK & PBI, and perform proton conductivity and other characterization analysis.
5) Prepare composite membrane based on ionic liquids and glycerol and testing their performances in fuel cell assembly.
6) Study the effect of ZrSi pH on proton conductivity and perform particle size distribution analysis.

References

[1] M. Jacobson, "Review of solutions to global warming, air pollution, and energy security," *Energy & Environmental Science*, vol. 2, pp. 148–173, 2009.

[2] A. Nesaraj, "Recent developments in solid oxide fuel cell technology–a review," 2010, Accessed: Dec. 05, 2020. [Online]. Available: http://nopr.niscair.res.in/handle/123456789/7374.

[3] G. Acres, "Recent advances in fuel cell technology and its applications," *Journal of Power Sources*, vol. 100, no. 1-2, pp. 60-66, 2001.

[4] Á. Varga, "Introduction to fuel cell technology," in *Fuel Cell Electronics Packaging*, pp. 1–32, 2007.

[5] U. Lucia, "Overview on fuel cells," *Renewable and Sustainable Energy Reviews*, vol. 30, pp. 164–169, 2014.

[6] X. Z. Yuan and H. Wang, "PEM fuel cell fundamentals," in *PEM Fuel Cell Electrocatalysts and Catalyst Layers: Fundamentals and Applications*, Springer London, 2008, pp. 1–87.

[7] C. Hartnig, L. Jörissen, W. Lehnert, and J. Scholta, "Direct methanol fuel cells," in *Materials for Fuel Cells*, 2008, pp. 185–208.

[8] L. Liu, W. Chen, and Y. Li, "An overview of the proton conductivity of nafion membranes through a statistical analysis," *J. Memb. Sci.*, vol. 504, pp. 1–9, Apr. 2016.

[9] M. Paidar, J. Mališ, K. Bouzek, and J. Žitka, "Behavior of Nafion membrane at elevated temperature and pressure," *Desalin. Water Treat.*, vol. 14, no. 1–3, pp. 106–111, 2010.

[10] R. E. Rosli *et al.*, "A review of high-temperature proton exchange membrane fuel cell (HT-PEMFC) system," *Int. J. Hydrogen Energy*, vol. 42, no. 14, pp. 9293–9314, Apr. 2017.

[11] A. F. Ghenciu, "Review of fuel processing catalysts for hydrogen production in PEM fuel cell systems," *Curr. Opin. Solid State Mater. Sci.*, vol. 6, no. 5, pp. 389–399, Oct. 2002.

[12] L. W. Niedrach, "The Performance of Hydrocarbons in Ion Exchange Membrane Fuel Cells," *J. Electrochem. Soc.*, vol. 109, no. 11, p. 1092, Nov. 1962.

[13] J. P. Hallett and T. Welton, "Room-temperature ionic liquids: Solvents for synthesis and catalysis. 2," *Chemical Reviews*, vol. 111, no. 5. pp. 3508–3576, May 11, 2011.

[14] E. H. E. Bayoumi, "Power electronics in smart grid distribution power systems: a review," *Int. J. Ind. Electron. Drives*, vol. 3, no. 1, p. 20, 2016.

[15] S. Mekhilef, R. Saidur, and A. Safari, "Comparative study of different fuel cell technologies," *Renewable and Sustainable Energy Reviews*, vol. 16, no. 1, pp. 981–989, Jan. 01, 2012.

[16] Y. Wang, K. S. Chen, J. Mishler, S. C. Cho, and X. C. Adroher, "A review of

polymer electrolyte membrane fuel cells: Technology, applications, and needs on fundamental research," *Applied Energy*, vol. 88, no. 4. Elsevier Ltd, pp. 981–1007, Apr. 01, 2011.

[17] H. Khakdaman, Y. Bourgault, and M. Ternan, "Direct propane fuel cell anode with interdigitated flow fields: Two-dimensional model," in *Industrial and Engineering Chemistry Research*, Feb. 2010, vol. 49, no. 3, pp. 1079–1085.

[18] N. Sammes, R. Bove, and K. Stahl, "Phosphoric acid fuel cells: Fundamentals and applications," *Curr. Opin. Solid State Mater. Sci.*, vol. 8, no. 5, pp. 372–378, Oct. 2004.

[19] Y. N. Sudhakar, M. Selvakumar, and D. K. Bhat, "Biopolymer Electrolytes for Fuel Cell Applications," in *Biopolymer Electrolytes*, vol. 5, no. 4, pp. 151–166, 2018.

[20] X. Chen, Y. Wang, Y. Zhao, and Y. Zhou, "A study of double functions and load matching of a phosphoric acid fuel cell/heat-driven refrigerator hybrid system," *Energy*, vol. 101, pp. 359–365, Apr. 2016.

[21] K. Mitsuda and T. Murahashi, "Air and fuel starvation of phosphoric acid fuel cells: A study using a single cell with multi-reference electrodes," *J. Appl. Electrochem.*, vol. 21, no. 6, pp. 524–530, Jun. 1991.

[22] P. Yang, H. Zhang, and Z. Hu, "Parametric study of a hybrid system integrating a phosphoric acid fuel cell with an absorption refrigerator for cooling purposes," *Int. J. Hydrogen Energy*, vol. 41, no. 5, pp. 3579–3590, Feb. 2016.

[23] J. Garche, C. Dyer, P. Moseley, Z. Ogumi, and D. Rand, *Encyclopedia of electrochemical power sources*, Fuel Cells - Alkaline Fuel cells | Overview Performance, pp. 321–328, 2009.

[24] A. L. Dicks, "Molten carbonate fuel cells," *Curr. Opin. Solid State Mater. Sci.*, vol. 8, no. 5, pp. 379–383, Oct. 2004.

[25] E. Arato, E. Audasso, L. Barelli, B. Bosio, and G. Discepoli, "Kinetic modelling of molten carbonate fuel cells: Effects of cathode water and electrode materials," *J. Power Sources*, vol. 330, pp. 18–27, Oct. 2016.

[26] W. He, "Dynamic performance of a reformer for molten carbonate fuel cell power-generation systems," *Fuel Process. Technol.*, vol. 53, no. 1–2, pp. 99–113, Nov. 1997.

[27] M. L. Perry and T. F. Fuller, "A Historical Perspective of Fuel Cell Technology in the 20th Century," *J. Electrochem. Soc.*, vol. 149, no. 7, p. S59, Jun. 2002.

[28] G. Merle, M. Wessling, and K. Nijmeijer, "Anion exchange membranes for alkaline fuel cells: A review," *Journal of Membrane Science*, vol. 377, no. 1–2. Elsevier, pp. 1–35, Jul. 15, 2011.

[29] Zulfirdaus Zakaria, Siti Kartom Kamarudin, "A review of quaternized polyvinyl alcohol as an alternative polymeric membrane in DMFCs and DEFCs," *International Journal of Energy Research*, vol. 44, no. 8, pp. 6223-6239, 2020.

[30] "Fuel Cell Systems Explained, 3rd Edition | Wiley." https://www.wiley.com/en-

us/Fuel/Cell/Systems (accessed Dec. 05, 2020).

[31] "Introduction to Transfer Phenomena in PEM Fuel Cells - 1st Edition." https://www.elsevier.com/books/introduction-to-transfer-phenomena-in-pem-fuel-cells/abderezzak/978-1-78548-291-5 (accessed Dec. 05, 2020).

[32] K. Sopian and W. R. Wan Daud, "Challenges and future developments in proton exchange membrane fuel cells," *Renew. Energy*, vol. 31, no. 5, pp. 719–727, Apr. 2006.

[33] "Recent Trends in Fuel Cell Science and Technology | S. Basu | Springer." https://www.springer.com/gp/book/9780387355375 (accessed Dec. 05, 2020).

[34] M. Díaz, A. Ortiz, and I. Ortiz, "Progress in the use of ionic liquids as electrolyte membranes in fuel cells," *Journal of Membrane Science*, vol. 469. Elsevier, pp. 379–396, Nov. 01, 2014.

[35] A. Mikolajczuk-Zychora *et al.*, "Highly active carbon supported Pd cathode catalysts for direct formic acid fuel cells," *Appl. Surf. Sci.*, vol. 388, pp. 645–652, Dec. 2016.

[36] M. Shao, "Palladium-based electrocatalysts for hydrogen oxidation and oxygen reduction reactions," *Journal of Power Sources*, vol. 196, no. 5. Elsevier, pp. 2433–2444, Mar. 01, 2011.

[37] M. Shao, "Electrocatalysis in Fuel Cells," *Catalysts*, vol. 5, no. 4, pp. 2115–2121, Dec. 2015.

[38] B. Cook, "Introduction to fuel cells and hydrogen technology," *Eng. Sci. Educ. J.*, vol. 11, no. 6, pp. 205–216, 2002.

[39] "Fuel Cell Technology Handbook - 1st Edition - Gregor Hoogers - Routle." https://www.routledge.com/Fuel-Cell-Technology-Handbook/Hoogers/p/book/9780367395773 (accessed Dec. 06, 2020).

[40] T. Wilberforce, A. Alaswad, A. Palumbo, M. Dassisti, and A. G. Olabi, "Advances in stationary and portable fuel cell applications," *Int. J. Hydrogen Energy*, vol. 41, no. 37, pp. 16509–16522, Oct. 2016.

[41] F. B. Spingler, A. Phillips, T. Schuler, M. C. Tucker, and A. Z. Weber, "Investigating fuel-cell transport limitations using hydrogen limiting current," *Int. J. Hydrogen Energy*, vol. 42, no. 19, pp. 13960–13969, May 2017.

[42] C. M. Kalamaras and A. M. Efstathiou, "Hydrogen Production Technologies: Current State and Future Developments," *Conf. Pap. Energy*, vol. 2013, pp. 1–9, 2013.

[43] O. Z. Sharaf and M. F. Orhan, "An overview of fuel cell technology: Fundamentals and applications," *Renewable and Sustainable Energy Reviews*, vol. 32. Pergamon, pp. 810–853, Apr. 01, 2014.

[44] Y. Wang, L. Li, L. Hu, L. Zhuang, J. Lu, and B. Xu, "A feasibility analysis for alkaline membrane direct methanol fuel cell: Thermodynamic disadvantages versus kinetic advantages," *Electrochem. commun.*, vol. 5, no. 8, pp. 662–666, Aug. 2003.

[45] P. K. Cheekatamarla, C. M. Finnerty, and J. Cai, “Internal reforming of hydrocarbon fuels in tubular solid oxide fuel cells,” *Int. J. Hydrogen Energy*, vol. 33, no. 7, pp. 1853–1858, Apr. 2008.

[46] R. Soltani, M. A. Rosen, and I. Dincer, “Assessment of CO2 capture options from various points in steam methane reforming for hydrogen production,” *Int. J. Hydrogen Energy*, vol. 39, no. 35, pp. 20266–20275, Dec. 2014.

[47] J. H. Wee, “Which type of fuel cell is more competitive for portable application: Direct methanol fuel cells or direct borohydride fuel cells?,” *Journal of Power Sources*, vol. 161, no. 1. Elsevier, pp. 1–10, Oct. 20, 2006.

[48] V. M. Vishnyakov, “Proton exchange membrane fuel cells,” *Vacuum*, vol. 80, no. 10, pp. 1053–1065, Aug. 2006.

[49] A. Al-Othman, Y. Zhu, M. Tawalbeh, A. Y. Tremblay, and M. Ternan, “Proton conductivity and morphology of new composite membranes based on zirconium phosphates, phosphotungstic acid, and silicic acid for direct hydrocarbon fuel cells applications,” *J. Porous Mater.*, vol. 24, no. 3, pp. 721–729, Jun. 2017.

[50] O. Savadogo and F. J. Rodriguez Varela, “Low-temperature direct propane polymer electrolyte membranes fuel cell (DPFC),” *J. New Mater. Electrochem. Syst.*, vol. 4, no. 2, pp. 93–97, Sep. 2001.

[51] A. S. Aricò *et al.*, “Investigation of grafted ETFE-based polymer membranes as alternative electrolyte for direct methanol fuel cells,” *J. Power Sources*, vol. 123, no. 2, pp. 107–115, Sep. 2003.

[52] E. Drioli, A. Regina, M. Casciola, A. Oliveti, F. Trotta, and T. Massari, “Sulfonated PEEK-WC membranes for possible fuel cell applications,” in *Journal of Membrane Science*, Jan. 2004, vol. 228, no. 2, pp. 139–148.

[53] L. Jörissen, V. Gogel, J. Kerres, and J. Garche, “New membranes for direct methanol fuel cells,” *J. Power Sources*, vol. 105, no. 2, pp. 267–273, Mar. 2002.

[54] M. Schulze and E. Gülzow, “Degradation of nickel anodes in alkaline fuel cells,” in *Journal of Power Sources*, vol. 127, no. 1–2, pp. 252–263, Mar. 2004.

[55] G. A. Koscher and K. Kordesch, “Alkaline methanol-air system: A historical survey and some new work,” *J. Solid State Electrochem.*, vol. 7, no. 9, pp. 632–636, 2003.

[56] J. Prabhuram and R. Manoharan, “Investigation of methanol oxidation on unsupported platinum electrodes in strong alkali and strong acid,” *J. Power Sources*, vol. 74, no. 1, pp. 54–61, Jul. 1998.

[57] S. C. Amendola, P. Onnerud, M. T. Kelly, P. J. Petillo, S. L. Sharp-Goldman, and M. Binder, “Novel high power density borohydride-air cell,” *J. Power Sources*, vol. 84, no. 1, pp. 130–133, Nov. 1999.

[58] M. Gao, X. Liu, M. Irfan, J. Shi, X. Wang, and P. Zhang, “Nickle-cobalt composite catalyst-modified activated carbon anode for direct glucose alkaline fuel cell,” *Int. J. Hydrogen Energy*, vol. 43, no. 3, pp. 1805–1815, Jan. 2018.

[59] T. Kuwabara and P. Kurzweil, “Fuel Cells - Phosphoric Acid Fuel Cells |

Anodes," in *Encyclopedia of Electrochemical Power Sources*, Elsevier, pp. 548–556, 2009.

[60] Y. Zhu, A. Y. Tremblay, G. A. Facey, and M. Ternan, "Petroleum Diesel and Biodiesel Fuels Used in a Direct Hydrocarbon Phosphoric Acid Fuel Cell," *J. Fuels*, vol. 2015, pp. 1–9, 2015.

[61] H. Su and Y. H. Hu, "Progress in low-temperature solid oxide fuel cells with hydrocarbon fuels," *Chemical Engineering Journal*, vol. 402. Elsevier B.V., p. 126235, Dec. 15, 2020.

[62] N. Yan, J. L. Luo, and K. T. Chuang, "Improved coking resistance of direct ethanol solid oxide fuel cells with a Ni-Sx anode," *J. Power Sources*, vol. 250, pp. 212–219, Mar. 2014.

[63] J. P. Trembly, A. I. Marquez, T. R. Ohrn, and D. J. Bayless, "Effects of coal syngas and H2S on the performance of solid oxide fuel cells: Single-cell tests," *J. Power Sources*, vol. 158, no. 1, pp. 263–273, Jul. 2006.

[64] R. J. Gorte, H. Kim, and J. M. Vohs, "Novel SOFC anodes for the direct electrochemical oxidation of hydrocarbon," *J. Power Sources*, vol. 106, no. 1–2, pp. 10–15, Apr. 2002.

[65] S. McIntosh and R. J. Gorte, "Direct hydrocarbon solid oxide fuel cells," *Chem. Rev.*, vol. 104, no. 10, pp. 4845–4865, Oct. 2004.

[66] F. Barbir, "Fuel Cell Electrochemistry," in *PEM Fuel Cells*, Elsevier, vol. 1, pp. 33–72, 2005.

[67] G. Kaur and G. Kaur, "Introduction to Fuel Cells," in *Solid Oxide Fuel Cell Components*, vol. 1, pp. 1–42, 2016.

[68] F.J. Rodríguez Varela, "Low-temperature direct propane polymer electrolyte membranes fuel cell (DPFC)," in *J. New Material*, vol. 4, no. 2, pp. 93–98, 2001.

[69] C. Boyer, S. Gamburzev, O. Velev, S. Srinivasan, and A. J. Appleby, "Measurements of proton conductivity in the active layer of PEM fuel cell gas diffusion electrodes," *Electrochim. Acta*, , pp. 3703–3709, Aug. 1998.

[70] *New materials for fuel cell systems I : proceedings of the First International Symposium New Materials for Fuel Cell Systems, Montréal, Québec, Canada, July 9 - 13, 1995*. Montréal: Editions de l'Ecole Polytechnique de Montréal, 1995.

[71] C. Yang, P. Costamagna, S. Srinivasan, J. Benziger, and A. B. Bocarsly, "Approaches and technical challenges to high temperature operation of proton exchange membrane fuel cells," *J. Power Sources*, vol. 103, no. 1, pp. 1–9, Dec. 2001.

[72] O. Savadogo, "Emerging membranes for electrochemical systems: Part II. High temperature composite membranes for polymer electrolyte fuel cell (PEFC) applications," in *Journal of Power Sources*, vol. 127, no. 1–2, pp. 135–161, Mar. 2004.

[73] Frantisek Marsík, "Detailed thermodynamic analysis of polymer electrolyte

membrane fuel cell efficiency" in *International Journal of Hydrogen Energy*, vol. 38, no. 17, pp. 7102–7113, June. 2013.

[74] J. Zhang, Y. Tang, C. Song, and J. Zhang, "Polybenzimidazole-membrane-based PEM fuel cell in the temperature range of 120-200 °C," *J. Power Sources*, vol. 172, no. 1, pp. 163–171, Oct. 2007.

[75] T. Wilberforce *et al.*, "Modelling and simulation of Proton Exchange Membrane fuel cell with serpentine bipolar plate using MATLAB," *Int. J. Hydrogen Energy*, vol. 42, no. 40, pp. 25639–25662, Oct. 2017.

[76] X. Huang, Z. Zhang, and J. Jiang, "Fuel cell technology for distributed generation: An overview," in *IEEE International Symposium on Industrial Electronics*, 2006, vol. 2, pp. 1613–1618.

[77] D. Ramdutt *et al.*, "Low energy plasma treatment of Nafion® membranes for PEM fuel cells," *J. Power Sources*, vol. 165, no. 1, pp. 41–48, Feb. 2007.

[78] S. Wen, C. Gong, W. C. Tsen, Y. C. Shu, and F. C. Tsai, "Sulfonated poly(ether sulfone) (SPES)/boron phosphate (BPO4) composite membranes for high-temperature proton-exchange membrane fuel cells," *Int. J. Hydrogen Energy*, vol. 34, no. 21, pp. 8982–8991, Nov. 2009.

[79] W. A. Siddiqui and S. A. Khan, "Synthesis, characterization and ion exchange properties of zirconium(IV) tungstoiodophosphate, a new cation exchanger," *Bull. Mater. Sci.*, vol. 30, no. 1, pp. 43–49, Feb. 2007.

[80] H. Sepehrian, A. R. Khanchi, M. K. Rofouei, and S. W. Husain, "Non-thermal synthesis of mesoporous zirconium silicate and its characterization," *J. Iran. Chem. Soc.*, vol. 3, no. 3, pp. 253–257, 2006.

[81] A. M. Abdelkader, A. Daher, and E. El-Kashef, "Novel decomposition method for zircon," *J. Alloys Compd.*, vol. 460, no. 1–2, pp. 577–580, Jul. 2008.

[82] H. Ye, J. Huang, J. J. Xu, N. K. A. C. Kodiweera, J. R. P. Jayakody, and S. G. Greenbaum, "New membranes based on ionic liquids for PEM fuel cells at elevated temperatures," *J. Power Sources*, vol. 178, no. 2, pp. 651–660, Apr. 2008.

[83] S. Gabriel and J. Weiner, "Ueber einige Abkömmlinge des Propylamins," *Berichte der Dtsch. Chem. Gesellschaft*, vol. 21, no. 2, pp. 2669–2679, Jul. 1888.

[84] M. Armand, F. Endres, D. R. MacFarlane, H. Ohno, and B. Scrosati, "Ionic-liquid materials for the electrochemical challenges of the future," *Nature Materials*, vol. 8, no. 8. Nature Publishing Group, pp. 621–629, 2009.

[85] M. Yoshizawa-Fujita, K. Johansson, P. Newman, D. R. MacFarlane, and M. Forsyth, "Novel Lewis-base ionic liquids replacing typical anions," *Tetrahedron Lett.*, vol. 47, no. 16, pp. 2755–2758, Apr. 2006.

[86] A. Ortiz, A. Ruiz, D. Gorri, and I. Ortiz, "Room temperature ionic liquid with silver salt as efficient reaction media for propylene/propane separation: Absorption equilibrium," *Sep. Purif. Technol.*, vol. 63, no. 2, pp. 311–318, Oct. 2008.

[87] M. Doyle, S. K. Choi, and G. Proulx, “High-Temperature Proton Conducting Membranes Based on Perfluorinated Ionomer Membrane-Ionic Liquid Composites,” *J. Electrochem. Soc.*, vol. 147, no. 1, p. 34, Jan. 2000.

[88] M. A. B. H. Susan, A. Noda, S. Mitsushima, and M. Watanabe, “Brønsted acid–base ionic liquids and their use as new materials for anhydrous proton conductors,” *Chem. Commun.*, vol. 3, no. 8, pp. 938–939, Apr. 2003.

[89] A. Fernicola, B. Scrosati, and H. Ohno, “Potentialities of ionic liquids as new electrolyte media in advanced electrochemical devices,” *Ionics*, vol. 12, no. 2. Springer, pp. 95–102, Jul. 27, 2006.

[90] M. Yoshizawa, W. Xu, and C. A. Angell, “Ionic Liquids by Proton Transfer: Vapor Pressure, Conductivity, and the Relevance of ΔpKa from Aqueous Solutions,” *J. Am. Chem. Soc.*, vol. 125, no. 50, pp. 15411–15419, Dec. 2003.

[91] B. Lin *et al.*, “Protic ionic liquid/functionalized graphene oxide hybrid membranes for high temperature proton exchange membrane fuel cell applications,” *Appl. Surf. Sci.*, vol. 455, pp. 295–301, Oct. 2018.

[92] H. Nakamoto, A. Noda, K. Hayamizu, S. Hayashi, H. O. Hamaguchi, and M. Watanabe, “Proton-conducting properties of a brønsted acid-base ionic liquid and ionic melts consisting of bis(trifluoromethanesulfonyl)imide and benzimidazole for fuel cell electrolytes,” *J. Phys. Chem. C*, vol. 111, no. 3, pp. 1541–1548, Jan. 2007.

[93] A. Noda, M. A. Bin Hasan Susan, K. Kudo, S. Mitsushima, K. Hayamizu, and M. Watanabe, “Brønsted acid-base ionic liquids as proton-conducting nonaqueous electrolytes,” *J. Phys. Chem. B*, vol. 107, no. 17, pp. 4024–4033, May 2003.

[94] J. Le Bideau, L. Viau, and A. Vioux, “Ionogels, ionic liquid based hybrid materials,” *Chem. Soc. Rev.*, vol. 40, no. 2, pp. 907–925, Jan. 2011.

[95] S. Thayumanasundaram *et al.*, “Hybrid inorganic-organic proton conducting membranes based on Nafion, SiO2 and triethylammonium trifluoromethanesulfonate ionic liquid,” *Electrochim. Acta*, vol. 55, no. 4, pp. 1355–1365, Jan. 2010.

[96] H. Li, F. Jiang, Z. Di, and J. Gu, “Anhydrous proton-conducting glass membranes doped with ionic liquid for intermediate-temperature fuel cells,” *Electrochim. Acta*, vol. 59, pp. 86–90, Jan. 2012.

[97] N. Shaari and S. K. Kamarudin, “Recent advances in additive-enhanced polymer electrolyte membrane properties in fuel cell applications: An overview,” *Int. J. Energy Res.*, vol. 43, no. 7, pp. 2756–2794, Jun. 2019.

[98] A. Al-Othman, A. Y. Tremblay, W. Pell, Y. Liu, B. A. Peppley, and M. Ternan, “The effect of glycerol on the conductivity of Nafion-free ZrP/PTFE composite membrane electrolytes for direct hydrocarbon fuel cells,” *J. Power Sources*, vol. 199, pp. 14–21, Feb. 2012.

[99] “Zircon Facts for Kids.” https://kids.kiddle.co/Zircon (accessed Dec. 06, 2020).

[100] J. E. Tsuchida, “Ionic conductivity and mixed-ion effect in mixed alkali

metaphosphate glasses," *Phys. Chem. Chem. Phys.*, vol. 19, no. 9, pp. 6594–6600, Mar. 2017.

[101] "1-Hexyl-3-methylimidazolium tricyanomethanide >98% | IoLiTec." https://iolitec.de/en/node/286 (accessed Dec. 06, 2020).

[102] "Diethylmethylammonium methanesulfonate, 98% | IoLiTec." https://iolitec.de/en/node/443 (accessed Dec. 06, 2020).

[103] "1-Butyl-3-methylimidazolium dicyanamide, >98% | IoLiTec." https://iolitec.de/en/products/ionic_liquids/catalogue/imidazolium-based/il-0010-hp (accessed Dec. 06, 2020).

[104] O. Zech, A. Stoppa, R. Buchner, and W. Kunz, "The conductivity of imidazolium-based ionic liquids from (248 to 468) K. B. variation of the anion," *J. Chem. Eng. Data*, vol. 55, no. 5, pp. 1774–1778, May 2010.

[105] "1-Ethyl-3-methylimidazolium methanesulfonate, 99% | IoLiTec." https://iolitec.de/en/node/99 (accessed Dec. 06, 2020).

[106] V. Di Noto *et al.*, "Influence of anions on proton-conducting membranes based on neutralized nafion 117, triethylammonium methanesulfonate, and triethylammonium perfluorobutanesulfonate. 2. electrical properties," *J. Phys. Chem. C*, vol. 116, no. 1, pp. 1370–1379, Jan. 2012.

[107] "1-Ethyl-3-methylimidazolium ethyl sulfate, 98% | IoLiTec." https://iolitec.de/en/node/94 (accessed Dec. 06, 2020).

[108] A. B. Pereiro, "Inorganic salts in purely ionic liquid media: The development of high ionicity ionic liquids (HIILs)," *Chem. Commun.*, vol. 48, no. 30, pp. 3656–3658, Mar. 2012.

[109] "1-Butyl-3-methylimidazolium thiocyanate, >98% | IoLiTec." https://iolitec.de/en/products/ionic_liquids/catalogue/imidazolium-based/il-0063-hp (accessed Dec. 06, 2020).

[110] K. Selvakumar, J. Kalaiselvimary, S. Rajendran, and M. R. Prabhu, "Novel Proton-Conducting Polymer Electrolytes Based on Poly(Vinylidene fluoride-co-hexafluoropropylene)–Ammonium Thiocyanate," *Polym. - Plast. Technol. Eng.*, vol. 55, no. 18, pp. 1940–1948, Dec. 2016.

[111] Zubeir, Lawien F., Rocha, Marisa A.A.,Vergadou, Niki, Weggemans, Wilko M.A., Peristeras, Loukas D. Schulz, Peter S., Economou, Ioannis G. Kroon, Maaike C., "Thermophysical properties of imidazolium tricyanomethanide ionic liquids: Experiments and molecular simulation," *Phys. Chem. Chem. Phys.*, vol. 18, no. 33, pp. 23121–23138, Aug. 2016.

[112] D. G. Kuroda, P. K. Singh, and R. M. Hochstrasser, "Differential hydration of tricyanomethanide observed by time resolved vibrational spectroscopy," *J. Phys. Chem. B*, vol. 117, no. 16, pp. 4354–4364, Apr. 2013.

[113] Catarina M.S.S., Kurnia, Kiki Adi, Coutinho, João A.P., Marrucho, Isabel M., Lopes, José N.Canongia, Freire, Mara G., Rebelo, Luís Paulo N., "Systematic study of the thermophysical properties of imidazolium-based ionic liquids with cyano-functionalized anions," *J. Phys. Chem. B*, vol. 117, no. 35, pp. 10271–

10283, Sep. 2013.

[114] “Glycerol, [Matrix for FABMS and liquid SIMS] | 56-81-5 | TCI-S0373 | Spectrum Chemical.” https://www.spectrumchemical.com (accessed Dec. 06, 2020).

[115] C. Y. Chen, S. L. Burkett, H. X. Li, and M. E. Davis, “Studies on mesoporous materials II. Synthesis mechanism of MCM-41,” *Microporous Mater.*, vol. 2, no. 1, pp. 27–34, Dec. 1993.

[116] H. Sepehrian, A. R. Khanchi, M. K. Rofouei, and S. W. Husain, “Non-thermal synthesis of mesoporous zirconium silicate and its characterization,” *J. Iran. Chem. Soc.*, vol. 3, no. 3, pp. 253–257, 2006.

[117] G. Anbalagan, A. R. Prabakaran, and S. Gunasekaran, “Spectroscopic characterization of indian standard sand,” *J. Appl. Spectrosc.*, vol. 77, no. 1, pp. 86–94, Mar. 2010.

[118] U. Kalapathy, A. Proctor, and J. Shultz, “A simple method for production of pure silica from rice hull ash,” *Bioresour. Technol.*, vol. 73, no. 3, pp. 257–262, Jul. 2000.

[119] A. Mbonyiryivuze, B. Mwakikunga, S. M. Dhlamini, and M. Maaza, “Fourier Transform Infrared Spectroscopy for Sepia Melanin,” *Phys. Mater. Chem.*, vol. 3, no. 2, pp. 25–29, Nov. 2015.

[120] K. Nishikida., “Infrared and Raman Analysis of Polymers”, *Mater. Sci.*, 2004.

[121] A. Samanta, K. Ojha, and A. Mandal, “Interactions between acidic crude oil and alkali and their effects on enhanced oil recovery,” *Energy and Fuels*, vol. 25, no. 4, pp. 1642–1649, Apr. 2011.

[122] M. A. Barique, E. Tsuchida, A. Ohira, and K. Tashiro, “Effect of Elevated Temperatures on the States of Water and Their Correlation with the Proton Conductivity of Nafion,” *ACS Omega*, vol. 3, no. 1, pp. 349–360, Nov. 2017.

[123] W. Binks, “The crystalline structure of zircon,” *Mineral. Mag. J. Mineral. Soc.*, vol. 21, no. 115, pp. 176–187, Dec. 1926.

[124] J. Liu, J. Song, T. Qi, C. Zhang, and J. Qu, “Controlling the formation of Na2ZrSiO5 in alkali fusion process for zirconium oxychloride production,” *Adv. Powder Technol.*, vol. 27, no. 1, pp. 1–8, Jan. 2016.

[125] G. Huang, Z. Pan, and Y. Wang, “Synthesis of sodium polyacrylate copolymers as water-based dispersants for ultrafine grinding of praseodymium zirconium silicate,” *Colloids Surfaces A Physicochem. Eng. Asp.*, vol. 558, pp. 591–599, Dec. 2018.

[126] P. Colomban and A. Novak, “Nature of the protonic species and the gel-crystal transition in hydrated zirconium phosphate,” *J. Mol. Struct.*, vol. 198, no. C, pp. 277–295, Jul. 1989.

[127] G. E. M. Jauncey, “The Scattering of X-Rays and Bragg’s Law,” *Proc. Natl. Acad. Sci.*, vol. 10, no. 2, pp. 57–60, Feb. 1924.

[128] Musyarofah, S. Soontaranon, W. Limphirat, Triwikantoro, and S. Pratapa, "XRD, WAXS, FTIR, and XANES studies of silica-zirconia systems," *Ceram. Int.*, vol. 45, no. 12, pp. 15660–15670, Aug. 2019.

[129] A. V. Anantaraman and C. L. Gardner, "Studies on ion-exchange membranes. Part 1. Effect of humidity on the conductivity of nafion®," *J. Electroanal. Chem.*, vol. 414, no. 2, pp. 115–120, Oct. 1996.

[130] Y. Devrim and A. Albostan, "Enhancement of PEM fuel cell performance at higher temperatures and lower humidities by high performance membrane electrode assembly based on Nafion/zeolite membrane," *Int. J. Hydrogen Energy*, vol. 40, no. 44, pp. 15328–15335, Nov. 2015.

[131] M. Amjadi, S. Rowshanzamir, S. J. Peighambardoust, M. G. Hosseini, and M. H. Eikani, "Investigation of physical properties and cell performance of Nafion/TiO2 nanocomposite membranes for high temperature PEM fuel cells," in *International Journal of Hydrogen Energy*, vol. 35, no. 17, pp. 9252–9260, Sep. 2010.

[132] M. B. A. Rahman, K. Jumbri, M. Basri, E. Abdulmalek, K. Sirat, and A. B. Salleh, "Synthesis and physico-chemical properties of new tetraethylammonium-based amino acid chiral ionic liquids," *Molecules*, vol. 15, no. 4, pp. 2388–2397, Apr. 2010.

[133] Y. Zhang and E. J. Maginn, "Direct correlation between ionic liquid transport properties and ion pair lifetimes: A molecular dynamics study," *J. Phys. Chem. Lett.*, vol. 6, no. 4, pp. 700–705, Feb. 2015.

[134] C. Schreiner, S. Zugmann, R. Hartl, and H. J. Gores, "Fractional walden rule for ionic liquids: Examples from recent measurements and a critique of the so-called ideal KCl line for the walden plot," *J. Chem. Eng. Data*, vol. 55, no. 5, pp. 1784–1788, May 2010.

Appendix

	Mass percentages (%)	Conductivities (S/cm)
	2.56	0.00051
	5.00	0.00042
ZrSi/[HMIM][TCM]	7.31	0.000159
	15.52	0.000325
	18.72	0.001282
	21.7	0.00745

	Mass percentages (%)	Conductivities (S/cm)
	5.3	0.0001979
	10.05	0.000141
ZrSi/[DEMA][OMS]	14.38	0.00135
	17.22	0.0001884
	22.14	0.00036
	26.23	0.00288
	30.01	0.00181
	32.74	0.00125

	Mass percentages (%)	Conductivities (S/cm)
	1.61	0.000197
ZrSi/[BMIM][DCA]	3.17	0.000117

	Mass percentages (%)	Conductivities (S/cm)
	3.22	0.000329
ZrSi/[EMIM][OMS]	4.42	0.000242
	6.20	0.00088
	8.65	0.00321

	Mass percentages (%)	Conductivities (S/cm)
	3.75	0.000697
ZrSi/[TEMA][OMS]	5.17	0.00012
	7.23	0.000145

	Mass percentages (%)	Conductivities (S/cm)
	0.71	0.00146
ZrSi/[BMIM][SCN]	1	0.002
	1.40	0.00164
	1.95	0.0013

	Mass percentages of GLY (%)	Conductivities (S/cm)
	0.157	0.0006
	0.34	0.00168
ZrSi/[HMIM][TCM] /GLY	0.469	0.196
	0.70	0.035
	1.11	0.028
	1.77	0.00306

	Mass percentages of GLY (%)	Conductivities (S/cm)
	0.18	0.0058
	0.387	0.1
ZrSi/[BMIM][SCN] /GLY	0.53	0.0323
	0.79	0.0129
	1.26	0.0097
	1.99	0.00455
	2.58	0.0005

	Mass percentages (%)	Conductivities (S/cm)
	1.17	0.00029
ZrSi/[EMIM][ESO_4]	1.64	0.000438
	2.32	0.00107
	3.23	0.00137

Vita

Rana Muhammad Nauman Javed was born in 1995, in Pakistan. He attended his primary and secondary education in the top institutes of Pakistan. He has professional experience in the industry as well as academic projects. In 2019, he joined the American University of Sharjah to pursue his master's degree from the department of chemical engineering. He has worked as a graduate teaching assistant.